Integrative spatial transcriptomic analysis pinpoints the role of TaMCO3 encoding ferroxidase in wheat root tip iron mobilization

Riya Joon[1,2], Gourav Singh[1], Deepshikha Tyagi[1,3], Varsha Meena[1], Vishnu Shukla[4], Kanupriya Agrwal[1,3], Hamida Banoo[1,2], Santosh Satbhai[5], Jagtar Singh[3], Terri Long[6], Eswarayya Ramireddy[4] and Ajay K Pandey[1*]

Author affiliations

[1]*National Agri-Food Biotechnology Institute (Department of Biotechnology), Sector 81, Knowledge City, S.A.S. Nagar, Mohali, Punjab, India*

[2]*Department of Biotechnology, Panjab University, Chandigarh, India*

[3]*Regional Centre of Biotechnology, Faridabad, India*

[4]*Indian Institute of Science Education and Research (IISER) Tirupati, Andhra Pradesh, India*

[5] Department of Biological Sciences, *Indian Institute of Science Education and Research (IISER) Mohali, India*

[6]*North Carolina State University, North Caroline, Raleigh, USA*

[*]*Corresponding author*

Dr. Ajay K Pandey, Scientist-F

National Agri-Food Biotechnology Institute (Department of Biotechnology), Sector 81, Knowledge City, Mohali-140306, Punjab, India.

Telephone: +91-1724990124

Email: pandeyak@nabi.res.in; pandeyak1974@gmail.com

ORCID iD: https://orcid.org/0000-0003-1064-139X

Summary

Iron (Fe) deficiency triggers molecular responses in plant roots, but the specific involvement of root tips in nutrient responses remains unclear. Therefore, in this study, we conducted a transcriptome analysis of wheat root tips under Fe deficiency, and a comparative transcriptome analysis was performed with the total root dataset. Gene ontology analysis highlighted the significance of oxidoreductase activity and metal/ion transport in the root tip tissue, which are critical for iron mobilisation. Interestingly, wheat displayed varying gene expression levels arising from the three genomes (A, B, and D) yet contributed to similar molecular functions. Detailed analysis of the oxidoreductase function in the root tip identified multiple multi-copper oxidase (MCO) proteins possibly contributing to the total ferroxidase activity. Detailed characterisation of Fe-responsive *TaMCO3* shows that it complements the yeast FET3 mutant and rescues the Fe-deficiency sensitivity phenotype of *Arabidopsis atmco3* mutants by enhancing vascular iron loading. Transgenic wheat lines overexpressing TaMCO3 exhibited increased root iron accumulation and improved tolerance to Fe deficiency by augmenting the expression of Fe-mobilizing genes. Our findings highlight the role of spatially resolved gene expression in Fe deficiency responses, suggesting strategies to reprogram cells for improved nutrient stress tolerance.

Keywords: iron, wheat, iron uptake, Ferroxidase, transcriptome, molecular functions

Introduction

Iron (Fe) is an essential micronutrient for plant growth development and plays a key role in regulating numerous cellular processes. Although Fe is present in the soil, it is primarily present in the insoluble Fe^{3+} form, which is not readily available to plants, thereby hindering the efficient uptake and mobilization of the plants. Low Fe availability in soil directly impacts plant productivity, with the onset of chlorosis in young leaves impacting the root architecture. Additionally, rhizospheric changes in other macro and micronutrient concentrations could also impact overall Fe assimilation. Consequently, plants rely on multiple strategies to enhance Fe solubilization and uptake from soil. Recent research has shown new insights on iron uptake *via* previously known Strategy I (reduction) and Strategy II (chelation) (Kobayashi and Nishizawa, 2012)–suggesting that plants adapt by selecting modules from both strategies based on environmental needs. For instance, dicots under alkaline soil conditions utilize a modified strategy I where Fe^{3+} reducing metabolites are secreted to facilitate Fe^{2+} uptake despite high pH and carbonate presence (Li *et al.*, 2023)

Non-graminaceous plants, such as *Arabidopsis*, use a reduction-based strategy (Strategy I) in which plasma-membrane (PM)-localized H^{+}-ATPases (AHAs) release protons to increase rhizosphere acidification and promote Fe^{3+} solubility. Subsequently, Fe^{3+} is reduced to the more soluble ferrous Fe^{2+} by ferric reduction oxidases (FROs) at the apoplast, and Fe^{2+} is transported into the root via the iron-regulated transporter (IRT1) (Santi and Schmidt, 2009). Graminaceous plants, including wheat, barley, and maize, utilize a chelation-based strategy (Strategy II). In this Strategy, plant roots secrete phytosiderophores (PS), forming Fe^{3+}-PS complexes in the rhizosphere. Fe^{3+}-PS is then taken up into root cells through the yellow stripe (YS) or yellow stripe-like (YSL) transporters for further long-distance transport (Curie *et al.*, 2009; Kobayashi *et al.*, 2010). The ability of plants to respond to soil nutrient availability is of fundamental importance for their adaptation to the

environment. Changes in root architecture can mediate the adaptation of plants to soils in which nutrient availability is limited by increasing the total absorptive surface of the root system. Under Fe deficiency conditions, roots can also mobilize Fe by releasing specialised, complex metabolites such as coumarins, PS and their derivatives, which facilitate Fe mobilization (Yi and Guerinot, 1996).

In general Fe deficiency largely resulted in decreased root growth with reduced biomass thereby affecting the overall architecture (Wang *et al.*, 2022). The molecular changes under Fe deficiency in roots were investigated in different plant including Arabidopsis, tomato, rice, wheat and maize, (Sun *et al.*, 2017; Martín-Barranco *et al.*, 2020; Molnár *et al.*, 2023; Gabay *et al.*, 2023a; Li *et al.*, 2016b; Chen *et al.*, 2022; Zanin *et al.*, 2017). Altogether, it was noted that the dynamic changes in the gene expression pattern remained temporal-specific yet specific transporters were identified that control Fe translocation between the subcellular compartments(Yokosho *et al.*, 2009; Conte and Walker, 2011). The root tip is the first part of the root that comes into contact with the changing dynamics of soil and is expected to play a critical role under nutrient stress. Therefore, the root apex represents the most probable site for sensing Fe limitation and excess (Baluška *et al.*, 1990). Accumulating evidence suggests that, compared to other regions of the root, the root tip is the most sensitive site for Fe fluctuation (Zhang *et al.*, 2012; Zhang *et al.*, 2011; Li *et al.*, 2016a; Li *et al.*, 2016c). Although previous studies have described the impacts of Fe deficiency on roots, little is known about root tip-specific responses (Kobayashi *et al.*, 2014; Schaaf *et al.*, 2005).

Once Fe is taken up by the root epidermal cells it is radially transported to the vasculature via the symplastic pathway and then exported into the vasculature system, especially xylem vessels, in the form of Fe^{2+}. It has been speculated that ferroportin (FPN)-like protein 1 is possibly involved in this process (Morrissey *et al.*, 2009). At this stage, it is

oxidized from Fe^{2+} to Fe^{3+} by plasma membrane-localized ferroxidases. Arabidopsis root tips exhibit high ferroxidase activity, mediated by AtLPR1, a multicopper (MCO) ferroxidase, which facilitates Fe mobilization under phosphate (Pi) deprivation (Xu *et al.*, 2022; Naumann *et al.*, 2022). AtLPR1 was also shown to participate in a module controlling root Fe accumulation that controls callose deposition (Müller *et al.*, 2015a). Similarly, OsLPR5 plays a significant role in plant growth and development in rice by regulating a subset of molecular components involved in Pi-homeostasis that control lateral root growth and grain filling (Ai *et al.*, 2020). At this stage Fe is transported as Fe^{3+}-citrate or Fe^{3+}-malate complexes. Thus, the ferroxidase activity of plant laccase type MCOs, such as LPR5, helps maintain Fe and Pi homeostasis and adapt to nutrient stress by enabling Fe redox cycling (Zhu *et al.*, 2022a; Hoopes and Dean, 2004a). Recent studies have shown that, it is the casparian strips in roots that are mainly responsible for selectively regulating nutrient absorption, blocking unregulated movement and enforcing symplastic or transcellular pathways. Especially at the root tip area, the polar localization of transporters that aids in efficient nutrient uptake by positioning specific transporters toward nutrient sources (Robe and Barberon, 2023). Thus, the plant tissue types facilitate the Fe uptake, transport, storage, and redistribution and maintain a balance to ensure optimal physiological functions and prevent toxicity.

Studying the role of root tips in crops under Fe deficiency can provide insights into early activation processes and reveal the specific activities that crops utilise to adapt to stress. Hexaploid wheat is an important source of energy and nutrition in many countries. Previously, the genome-wide transcriptome was generated from the roots of wheat seedlings that served as an inventory of Fe-responsive genes (Kaur *et al.*, 2019; Wang *et al.*, 2019; Kaur *et al.*, 2023). In the current study, we specifically examined transcriptional responses of the hexaploid wheat root tip. We identified the wheat ferroxidase candidate gene, TaMCO3, and characterized its role in iron mobilisation and deficiency response. Altogether, this work

highlights the importance of tissue-type specific iron deficiency-responsive genes in the root tips of hexaploid wheat that could serve as targets for modifying cellular behaviour under nutrient stress.

Results

Root tip transcriptome analysis identifies "representative-core Fe deficiency response"

Previously, it was demonstrated that root tips (meristematic zone) are the primary site of Fe-sensing. Therefore, we performed RNAseq analysis of wheat root tips (crown, seminal and primary roots) exposed to optimal +Fe (control) and –Fe to gain further insight into how these conditions impact transcriptional responses. To validate experimental conditions the roots from these experiments were treated with Perls/DAB staining **(Figure 1A)**. The low accumulation of Fe in the root tips suggested that the wheat seedlings experienced –Fe conditions compared to the control. We were able to mapped more than >90% of the reads generated in the transcriptome, and it was submitted to NCBI (BioProject ID: PRJNA1178603). We observed a wide dispersion of gene expression from the two treatments **(Figure 1B),** with the highest Log2FoldChange (Log2FC) ranging from +8.0 (upregulated) to -6.6 (downregulated). A total of 6234 genes were differently expressed (LogFC>1.0) in response to –Fe (**Table S1**). Out of this 4805 genes were upregulated, and 1429 genes were downregulated I **(Figure 1C)**. Next, we performed the comparative molecular expression analysis of root tips with the previously published whole root transcriptome (4 and 8 D (days) of –Fe) data set (Kaur *et al.*, 2023). Interestingly, we observed that 377 genes are commonly expressed at all the data points and in root tips (**Table S1**); whereas 5036 DEGs were noted for "root-tip specific" responses. Out of the total DEGs, 567 genes was found to be common between 8D root and root tip DEGs subjected to –Fe.

Comparative transcriptome analysis of root tip and whole root under Fe deficiency

Next, we compared the DEGs pertaining to Fe homeostasis responses for different time points of –Fe. In general, in both the data sets we found that genes encoding Nicotinamine acid synthase (NAS) and Nicotianamine aminotransferase (NAAT) proteins are highly induced by –Fe (**Table S1**). Various transporters, including Zinc-induced facilitator-like (ZIFL) protein-encoding genes known to be involved in PS release, were also highly upregulated. Additionally, YSL genes were highly represented in the RNAseq data set **(Figure 2A)**. Multiple transcription factors including the basic-helix-loop helix (bHLH) family genes those were reported earlier were also highly represented in our dataset **(Figure S1A** and **B)**. Overall, our data reveal that the expression of genes in the wheat root tip represents the "representative-core Fe deficiency response".

Next, we performed comparative GO annotation distribution for the DEGs specific to the root tip and common DEGs (root-tip and whole root-8D). For root-tip, our analysis reveals enrichment of GO terms such as "response to oxidative stress", "response to metal ions", "metal ion transport", and other related functions (**Figure 2B** and **Table S2**). A comparative GO annotation was also performed for the genes commonly identified between root-tip and root DEGs datasets (**Table S3**). Interestingly, both the GO annotations shared multiple key terms. The comparative GO annotation showed enrichment in terms such as response to ethylene, oxidative stress, iron transport, response to metals and organic acid metabolism (**Figure 2B**). For this analysis, we observed that although many of the GO terms overlapped among these datasets, in general, we observed the higher proportion of genes in the root-specific response when compared to the shared genes dataset for a similar biological process.

Oxidoreductase activity is the major contributor at the root tip

Next, we checked the distribution of the A, B and D genome transcripts towards the GO functions. In general, we observed that although the number of genes varies among the homoeologs, the nature of GO functions was very similar for the genes derived from either genome (**Figure 3A and Table S4**). We observed that DEGs associated with the GO category, response to hormone, represented the largest contribution of DEGs across the sub-genome. It was notable that genes within the GO category "oxidation-reduction process" were highly enriched in the pericycle transcript encoded by A and B genomes. Further detailed analysis of this category of genes revealed many genes encoding for Laccases-like Multi-Copper Oxidases (MCOs). MCOs are glycoproteins that catalyse the oxidation of various substrates, including Fe, to modulate root-to-shoot Fe partitioning (**Figure 3B and Table S5**). Heat map analysis of wheat MCOs suggested that a specific cluster of MCOs genes are differentially expressed in the root tip in response to 4 and 8 days of –Fe . In addition to this we observed differential expression of peroxidases encoding transcript but no expression was observed for ferric chelate reductase (**Figure S2**). This analysis suggests that wheat MCOs are possibly involved in iron mobilization in a tissue-type-specific manner via its ferroxidase activity.

TaMCO3 complements the yeast FET3 ferroxidase function

In yeast, the multicopper oxidase FET3 operates as a ferroxidase, converting Fe^{2+} to Fe^{3+}, which is essential for iron absorption (Hoopes and Dean, 2004a). To identify the closest ortholog of FET3 in wheat, we conducted an extensive phylogenetic analysis of genes induced by iron deficiency that encode MCOs **(Figure 4A)**. The percentage identify of FET3 with wheat MCOs ranges from 19-30% (**Figure S3**). Among these candidates, TraesCS5A02G286900, referred to as TaMCO3-5A, was significantly upregulated across all tested iron deficiency conditions and was identified as the closest homolog to FET3. Next, we

checked the expression of representative MCOs (*TraesCS6D02G361500*, *TraesCS7D02G176300*, *TraesCS1D02G044300*, *TraesCS3A02G452600*, *TraesCS5A02G286900* and *TraesCS4D02G035000)* from all the clades. Our expression analysis under –Fe indicated that all the TaMCOs showed higher expression on 8D compared to 4D. Interestingly, upon resupply of Fe, *TraesCS6D02G361500*, *TraesCS1D02G044300*, *TraesCS3A02G452600* and *TraesCS4D02G035000* show higher expression when compared to control or –Fe conditions (**Figure 4B**). Two TaMCOs viz. *TraesCS7D02G176300* and *TraesCS5A02G286900* show significantly higher expression at 4D of –Fe and remained unaffected by resupply at 8D. Given the *TraesCS7D02G176300* and *TraesCS5A02G286900* are early expressed and show similar expression patterns, we selected these two genes for further studies. Domain analysis and percentage identity of *TraesCS7D02G176300* (27.89%) and *TraesCS5A02G286900* (28.97%) with ScFet3 showed conserved cupredoxin and ascorbate oxidase domains, while plasma membrane domain was missing in wheat proteins (**Figure S3** and **Figure 5A**). *TraesCS5A02G286900* (*TaMCO3*) show the highest expression in root tip among all the MCOs and also falls in the same clade along with FET3.

Firstly, we examined the expression of *TaMCO3* in roots under different Fe availability conditions and found increasing fold change in transcript levels under deficient conditions (0, 0.1, and 1 µM Fe) when compared to the control (80 µM Fe). We also observed that the expression of *TaMCO3* decreased with increased Fe levels. This highlights that the expression response to *TaMCO3* depends on the Fe availability **(Figure 5B)**. Furthermore, considering the possible redox fluctuations in roots driven by pH, we assessed *TaMCO3* expression levels at various pH conditions. The gene showed greater expression at low pH compared to a more neutral pH of 6.5, likely due to redox shifts that influence iron availability in the rhizosphere **(Figure 5C)**. For functional characterization, we investigated

whether TaMCO3 (TaMCO3-5A) could compensate for the functionality of yeast FET3. We fused the open reading frame (ORF) of TaMCO3 to the plasma membrane (PM) anchoring domain of yeast FET3. In yeast, the PM-anchored TaMCO3 successfully alleviated the iron sensitivity phenotype of the fet3 mutant (Brun *et al.*, 2022), localizing to the plasma membrane and restoring ferroxidase activity **(Figures 5D, E and F)**. This strongly suggests that TaMCO3 serves a similar role in iron oxidation as FET3 does in yeast. Additionally, we broadened our investigation by evaluating the role of TaMCO3 in Arabidopsis *atmco3* mutants and hexaploid wheat to gain further insights into its function.

TaMCO3 complements Arabidopsis mutant and contributes to iron deficiency tolerance

To investigate the subcellular localization of TaMCO3, we transiently expressed TaMCO3-YFP in *Nicotiana benthamiana* leaves using agro-infiltration. Our findings indicated that the TaMCO3-5A fusion protein primarily localized to the periplasmic space and the plasma membrane in tobacco leaf cells **(Figure 6A)**. This localization was supported by similar results obtained in yeast cells, where TaMCO3 also localized to the plasma membrane **(Figure 5E)**, suggesting that subcellular targeting may be conserved across species. In addition to the localization study, we assessed the functional activity of TaMCO3 in relation to iron deficiency.

Previously, it was shown that (Bernal and Krämer, 2021). Based on this evidence, we proposed that TaMCO3 could play a pivotal role in iron mobilization and uptake in conditions of iron scarcity. To evaluate this hypothesis, we generated multiple *atmco3* lines overexpressing MYC:TaMCO3. Two independent transgenic lines with high protein expression were selected for further physiological analysis (**Figure S4**). Our phenotypic assessment showed that under +Fe, the root lengths of Col-0, *atmco3* mutants, and the TaMCO3-complemented lines exhibited no significant differences **(Figure 6B and Figure**

S4). However, under –Fe, the *atmco3* mutants displayed a significant decrease in root growth, indicating an increased sensitivity to low iron levels. Across different TaMCO3 complemented lines, the root lengths were comparable to those of Col-0, suggesting that the overexpression of TaMCO3 effectively rescued the iron deficiency phenotype in the *atmco3* mutant **(Figure 6B and C, Figure S4).** To further examine the role of TaMCO3 in iron accumulation, we quantified the iron content in the roots of these Arabidopsis lines using inductively coupled plasma mass spectrometry (ICP-MS). Our results demonstrated that the TaMCO3 overexpressing lines were capable of restoring iron accumulation in the roots to levels similar to those of Col-0, whereas the *atmco3* mutants exhibited significantly lower iron accumulation **(Figure 6D and E)**. This indicates that TaMCO3 is engaged in the iron uptake process in wheat, and its overexpression in Arabidopsis can compensate for the functional loss in the *atmco3* mutant.

Additionally, our results were supported by Perl's staining, which specifically detects Fe^{3+} in plant tissues. The staining patterns revealed a significant restoration of iron uptake in the TaMCO3 complemented lines, while the *atmco3* mutants exhibited reduced iron uptake, further reinforcing the role of *TaMCO3* in Fe homeostasis **(Figure 6E)**. Under –Fe condition the expression of *IRT* and *FRO2* in TaMCO3 complemented lines showed a similar expression response as observed in Col-0 **(Figure 6F and G)**. Overall, these findings suggest that TaMCO3 plays a crucial role in iron mobilization and uptake, particularly under –Fe conditions, thereby helping to alleviate symptoms of iron deficiency in both Arabidopsis and wheat.

Overexpression of TaMCO3 contribute to iron deficiency tolerance

Next, we went on to characterize wheat *TaMCO3* using the ExVip expression database (Ramírez-González *et al.*, 2018) at different Zadosky scale (Z) that indicated high expression

of *TaMCO3* in the roots (Z13 and Z39 stage) compared to other wheat tissues (**Figure 7A)**. The expression of TaMCO3 was also post few days after anthesis (DAA) and grain tissue. Our qRT-PCR expression data suggest highest expression at 28 DAA and highest expression was noted in pericarp tissue (**Figure S5**). Previously root tip transcriptome was done in monocot-specific *12-OXOPHYTODIENOATE REDUCTASE* (OPRIII) overexpression lines of wheat that were shown to modulate key differences in wheat root architecture (Gabay *et al.*, 2023b). The expression *TaMCO3* was found to be high in the transgenic lines and specifically in the root tip (**Figure 7B**). Together these data suggest that some MCO ferroxidases may be root-specific. Next, we assessed wheat root ferroxidase activity by growing plants in the presence of $FeSO_4$ (as the only Fe source), and quantifying ferrous iron chelation to ferrozine as a proxy for ferroxidase activity. Our results show that within days of exposure to Fe_2SO_4 there is a decrease in ferrozine-Fe^{2+} complexes, (**Figure 7C**), suggesting high oxidation activity. We then tested the total ferroxidase activity in wheat roots under iron-sufficient and deficient conditions, and observed a significant disappearance of ferrozine-Fe^{2+} complexes in roots subjected to Fe deficiency (**Figure 7D**). This supports the earlier notion of generation of Fe^{3+} forms in the vascular system, which is chelated with citrate/malate for long distance movement of Fe.

In order to assess its function further, we overexpressed TaMCO3 in wheat *cv*. Fielder using a constitutive promoter. Immature embryos were used to generated wheat transgenic lines (**Figure S6A**).We generated seven transgenic lines, and characterized in two transgenic lines (**Figure S6B:** Line#2, #4**)**. The c-MYC immunoassay of the transgenic lines expressing c-MYC:TaMCO3 suggested its uniform localization onto the plasma membrane of the root tissue types **(Figure 7E)**. This localization was consistent across the independent transgenic lines (**Figure S7**). Next, these transgenic lines were assayed for Fe deficiency response. We found that TaMCO3 overexpression causes delayed young leaf chlorosis compared to WT, as

evident by decreased SPAD values **(Figure 7F)**. Interestingly, overexpressing lines show no change in the root architecture whereas the WT shows reduced root growth under Fe deficiency conditions **(Figure S8A)**. Subsequently, we measured the Fe accumulation in the root and shoot of transgenic and non-transgenic wheat. Under control conditions, higher Fe levels were observed in transgenic lines both the root and shoot respectively when compared to the non-transgenic (WT) **(Figure 7G and Figure S8C)**. Surprisingly, under –Fe condition both transgenic and WT lines show no-significant differences of Fe; whereas, in shoot significantly high Fe levels were measured in the transgenic lines. We speculate that the elevated Fe in the shoots of these overexpression lines it due to increased translocation from the root to the shoot due to high ferroxidase activity. At the molecular level we also checked the expression of known Fe responsive genes. Our analysis suggests that while none of our candidate genes are differentially expressed under +Fe, but during –Fe treatment, *TaYS1A* expression was elevated in *TaMCO3* overexpression transgenic lines compared to WT. No significant changes in the expression of *TaIRT1*, *TaIRO3*, *TaFIT, and TaNAS3* was observed in the transgenic lines subjected to –Fe condition. Interestingly, high expression of *TaZIFL4.1*, *TaIRT1*, *TaIRO3*, *TaFIT, and TaNAS3* in WT under –Fe when compared to +Fe **(Figure 8A)**. This suggests high uptake of Fe in roots and contributes to delayed chlorosis in TaMCO3-transgenic wheat.

Discussion

The root tip is a sensory hub, that detects environmental signals, including nutrient fluctuations, They enable plants to adapt varying soil conditions by altering root growth direction or rate (Zhang *et al.*, 2018; Jiang *et al.*, 2016) via transcriptional and translational regulatory processes that control root tropisms, cell polarity, and cell fate (Baluška *et al.*, 1990). Our previous transcriptomic analysis of wheat roots subjected to Fe deficiency

identified genes involved in its mobilization and uptake (Kaur *et al.*, 2019; Kaur *et al.*, 2023). Multiple biochemicals such as organic acids such as citrate and malate were also shown to accumulate in high amounts in the roots undergoing Fe deficiency (Kaur *et al.*, 2019). In addition, the amount of PS released by the root tips plays a critical role in deficiency tolerance in hexaploid wheat (Meena *et al.*, 2024). However, these studies have primarily focused on the total root response, thereby limiting our understanding of the sensing-hub site of the wheat root i.e. root tip. Our current study focuses on understanding the molecular mechanisms of how hexaploid wheat root tips respond to iron deficiency. Root tips are likely the primary site for detecting and responding to heterogenous iron fluctuations in the rhizosphere (Li *et al.*, 2016b). Our transcriptomics analysis of the root tip proves that this region represents the site of core Fe deficiency sensing and response **(Figure 2A)**. Detailed analysis identified specific GO annotations, related to genes encoding for iron/metal mobilisation and oxidoreductase activities.

Fe is present in soil in different forms primarily governed by soil conditions, including pH and redox status. Soil iron is mainly present in the two most common oxidation states, Fe^{2+} and Fe^{3+}, which interact with other elements and minerals to determine their availability to plants. Under nutrient deficiency conditions, plant root tips maintain homeostatic redox balance to coordinate normal development. The overall redox status of specific root zones under nutrient-limiting conditions or during abiotic stresses helps plants cope with stresses. For example, in Arabidopsis, varying redox potential has been observed in the root zones undergoing salinity stress (Jiang *et al.*, 2016). Our study observed a large set of genes encoding for the GO annotations related to the oxidoreductase/oxidation-reduction activity/process **(Figure 3B)**. It is imperative that plants undergoing iron stress primarily rely on the redox potential of the cell to fine-tune its response. Earlier, the root spatial expression of –Fe responsive genes was dissected at the cell-layer–specific and inter–cell-layer (Dinneny

et al., 2008). The importance of such studies to the abiotic stresses shall assist in rationalizing developmental clues during the changing environments. Altogether, our study utilizes the spatial transcriptome analysis of the root tip data set that pinpointed the tissue type necessary for iron mobilisation and how the dataset could be used to identify the genetic redundancies of the wheat genome for specific functions. Elucidating how root tip respond to Fe deficiency will significantly help improve our understanding of how plants adapt to metal stresses, including iron.

Understanding the spatial distribution of the Fe deficiency-induced genes is vital as this could help distinguish the core set of genes that may arise across the cell or tissue type towards specific responses. Our investigation of –Fe DEGs to the previous known dataset revealed that redox homeostasis processes is one of the most prevalent GO categories associated with genes differentially regulated in the wheat root tip (**Figure 3B**). This led us to identify multiple MCOs encoding ferroxidases potentially involved in efficient Fe mobilisation. Human MCOs have been identified and characterized to be ceruloplasmin proteins that possess ferroxidase activity regulating the Fe turnover by oxidizing ferrous from Fe(II) to ferric Fe^{3+} (Vashchenko and MacGillivray, 2013). Similarly, in lower eukaryotes like yeast, the MCO, FET3, was demonstrated to be a ceruloplasmin homolog showing ferroxidase activity (Stoj and Kosman, 2003). At the functional level, the cell-surface activity of FET3 is required for high-affinity transport of Fe (De Silva *et al.*, 1995). Previously, 17 plant laccase-like MCOs were characterized in detail in Arabidopsis showing diverse tissue-specific expression patterns at distinct stages the plant development (Turlapati *et al.*, 2011). Our phylogenetic analysis of the MCOs shows a specific cluster responding to the Fe deficiency-induced expression **(Figure 3)**. A detailed analysis reveals that wheat gene ID *TraesCS5A02G286900* (TaMCO3-5A) is closest to *Saccharomyces cerevisiae* FET3. Ferroxidases are known to be expressed mainly in the pericycle membrane and are reported

375 to generate Fe^{3+} from thereby facilitating the mobilization of Fe^{3+}-chelate forms (Bernal and
376 Krämer, 2021; Liu *et al.*, 2022; Zhu *et al.*, 2022b). In our study we found that TaMCO3-YFP
377 is localized to the plasma membrane and overexpression of TaMCO3 likely leads to
378 increased ferroxidase activity. Consequently, it reduces chlorotic response and thereby
379 indirectly modulates the expression of Fe acquisition gene when exposed to its deficiency
380 **(Figure 7F and Figure 8A)**. This finding correlate with the observed high shoot Fe in the
381 transgenic lines compared to WT thereby providing resistance to Fe deficiency in the
382 rhizosphere. On the similar lines, high ferroxidase activities in rice is also linked to enhanced
383 grain Fe content that could be attributed to the high mobilization capacity of the iron to the
384 grain tissue (Gu *et al.*, 2024). Recently, rice OsLPR5 was shown to be linked with
385 modulating salt stress and Fe homeostasis-related genes (Ai *et al.*, 2020; Zhao *et al.*, 2023).
386 This interconnection with salt and iron stress was attributed mainly to the redox changes in
387 the plant roots. Together, these findings suggest that TaMCO3 in wheat root tips may be
388 important for sensing –Fe and oxidizing Fe^{2+} for mobilization to the root **(Figure 6B)**.
389 Consequently, overexpression of TaMCO3 results in robust root growth even under
390 Fe deficiency conditions, compared to WT **(Figure S7)**. This suggests that the presence of
391 high ferroxidase also contributes to root growth and biomass. Previously, another MCO,
392 LPR1 was linked to iron-dependent callose deposition in response to low phosphate
393 conditions (Müller *et al.*, 2015b). Localization of the MCOs has been linked to the cell wall
394 maintenance and overexpression has been linked with the high Fe^{3+} in both roots and shoots
395 (Bernal and Krämer, 2021). In our overexpressing lines TaMCO3 protein was expressed
396 constitutively expressed on the plasma membrane on different cell types. As a result the
397 overexpression of TaMCO3 leads to high accumulation of iron in shoots and roots **(Figure**
398 **7G)**. Such high accumulation might be beneficial for enhanced iron loading in the xylem,

and subsequently into seeds using tissue-specific endosperm promoters fused to iron-transporters, or for imparting Fe deficiency tolerance to growing wheat seedlings.

Based on the evidences presented in this work we propose a model reflecting the importance of the different cluster for the DEGs that could be the bottleneck checkpoints for Fe loading in specific cell/tissue type (**Figure 8B**). Overall, the gene contributing to the strategy II mode of Fe uptake is constitutively expressed and the expression of these genes are high with the –Fe condition. At the sub-genome derived gene expression level although the contribution by differ yet they all contribute to similar biological process. As evident form the results, the wheat MCO3 localized in the plasma-membrane plays an important role for generating Fe^{3+} so as to mobilize Fe to shoots. One of the limitations of this study is performing the cell type analysis in wheat roots directly under Fe deficiency conditions or other essential hub genes regulating iron responses such as proteins involved in the sensing of iron or bHLH iron regulators. Nonetheless integrating the knowledge of the specialized region of the "root tip" should provide the much-needed missing insight at the mechanistic level.

Materials and methods

Plant material and growth conditions

The hexaploid wheat cv. C-306 and Fielder were selected for experiments. Wheat seeds were stratified overnight in the dark at 4 °C and then germinated on Petri dishes lined with Whatman filter paper. Endosperms were removed from 4-day old seedlings, which were subsequently transferred to PhytaBox™ containers, where they were cultivated using Hoagland's nutrient solution. For iron deficiency (–Fe), 1 µM Fe^{3+}-EDTA was used, while control plants (+Fe) received 80 µM Fe^{3+}-EDTA without altering other nutrient concentrations. The plants were grown in a controlled growth chamber set at 21±1°C, with

50–65% relative humidity, and a photon flux density of 300 µmol m^{-2} s^{-1}, under a 16-hour light/8-hour dark photoperiod. Roots and shoots were harvested from three biological replicates after 8 days post-deficiency and immediately frozen in liquid nitrogen for subsequent analysis. For root tip RNAseq analysis, the root tips were collected up to ~2.5mm from the apex portion (containing the meristematic zone). Total RNA was extracted from the tissue from the three biological replicates and was processed for transcriptome analysis as described earlier (Kaur *et al.*, 2019; Kaur *et al.*, 2023).

Bioinformatic and GO enrichment analysis

Transcriptome analysis followed the method described earlier (Kaur *et al.*, 2019; Kaur *et al.*, 2023). Data was generated from three biological replicates for each treatment. Trimmomatic 0.35 was used to trim and filter reads, discarding those with a Phred score below Q20. Cleaned reads were mapped to the reference genome (IWGSC_RefSeq_v2.1) using TopHat v2.1.1, and Cufflinks v2.2.1 was used for transcript assembly and expression quantification. Genes with a Log2FC>1.0 were considered upregulated, and those with Log2FC<1.0 were downregulated. Differentially expressed genes (DEGs) were identified based on statistical significance ($P < 0.05$) and a false discovery rate ($FDR < 0.05$). The gene ontology (GO) enrichment of DEGs (Log2FC>1.0) and clusters genes was performed using the AgriGO v2 (Tian *et al.*, 2017) based on the Fisher test and the GO enrichment plots were generated using ggplot2 in the R program. The plant TFs were predicted from DEGs using iTAK program version 1.7 (https://itak.feilab.net/) with default parameters (Zheng *et al.*, 2016). For the Heatmap generation, the normalized Log2FC was plotted using TB Tools software (Chen *et al.*, 2020).

Arabidopsis complementation and experimental conditions

The *TaMCO3* ORF (2019 bp; *TraesCS5A02G286900* highly expressing) was cloned into the plant expression vector pGWB520. The resulting construct was introduced into *Arabidopsis thaliana atmco3* mutant lines (SALK_039183) through *Agrobacterium tumefaciens*-mediated transformation using the GV3101 strain. Following transformation, T_1 generation seeds were screened for hygromycin resistance (20 µg/ml), and true transformants capable of reaching the four-leaf stage were selected. These plants were then transferred to soil pots and allowed to grow to maturity. T_2 generation seeds were harvested, and the subsequent T_2 plants were cultivated to obtain T_3 seeds. Upon confirmation of successful transformation, Arabidopsis seeds from Col-0, *atmco3*, and TaMCO-complemented lines were germinated and grown in Hoagland media for 5 days under control conditions. For phenotypic assays and the seedlings were transferred to three different iron treatments for 8 days: (i) with 80 µM FeEDTA (+Fe), (ii) without iron and with 300 µM ferrozine (–Fe), and (iii) with 300 µM FeEDTA (+++Fe) to induce iron toxicity. All the assessment and processing of the samples were done after 7 days of growth on the indicated plates.

Perls and Ferrozine Staining in roots

Wheat plants (*Triticum aestivum*) and *Arabidopsis thaliana* seedlings were grown in a controlled environment using Hoagland's nutrient solution, supplemented with 40 µM Fe_2SO□ and 60 µM Na-EDTA to maintain optimal iron supply. Upon reaching the desired developmental stage, root samples were collected to assess Fe^{2}□ accumulation using two distinct staining techniques: Ferrozine staining and Perl's Prussian Blue staining. For Fe^{2}□ detection, the roots were incubated in a freshly prepared 100 µM ferrozine solution. To ensure effective penetration, the samples underwent vacuum infiltration for 1 hour in complete darkness, minimizing the potential degradation of the ferrozine-Fe^{2}□ complex. Following the infiltration, roots were thoroughly rinsed with deionized water to remove

excess stain and then examined under a stereomicroscope for Fe^{2+} localization. In parallel, Perl's Prussian Blue staining was employed to detect Fe^{3+} ions. Root samples were immersed in a solution containing 5% potassium ferrocyanide and 5% HCl and vacuum infiltrated under dark conditions for 1 hour to enhance reagent penetration. After staining, roots were carefully washed with deionized water to remove any unbound stain, and the presence of Fe^{3+} was visualized by the formation of a blue precipitate. Following this, for DAB staining of wheat roots a thorough washing with distilled water was done to remove any excess staining (Perl's) solution. Furthermore, the plants were kept in freshly prepared solution composed of 0.1% DAB (3,3'-Diaminobenzidine) in 0.1 M Sodium citrate buffer, pH 3.8 under dark conditions. A final rinse with distilled water was done to remove any residual dye. All DAB, ferrozine- and Perl-stained roots were examined and imaged under a stereomicroscope to document the distribution of Fe^{2+} and Fe^{3+} ions across different root zones.

Yeast complementation assay

A yeast complementation assay was performed using the *S. cerevisiae* mutant strain *fet3fet4*, deficient in iron uptake, to test the function of wheat *TaMCOs*. The coding sequences of multiple wheat MCO were cloned into the pYES2 expression vector, generating two constructs: *TaMCOs-pYES2* and *TaMCO-PM-pYES2* (the latter containing the plasma membrane-PM domain of yeast *FET3*). These constructs were transformed into *S. cerevisiae* wild-type BY4741 and *fet3fet4* strains via the lithium acetate method. Transformed cells were selected on SD -Ura medium and their growth was assessed by spotting serial dilutions onto DOB -Ura plates under two conditions: iron-sufficient (50 mM MES and 100 μM ferric citrate) and iron-deficient (50 mM MES only). The assay evaluated the ability of *TaMCOs* to complement the iron uptake deficiency in *fet3fet4* mutants.

In-silico identification of wheat MCOs genes and Phylogenetic analysis

To analyse the phylogenetic relationship between yeast *fet3* and wheat, *Arabidopsis*, *O. sativa* MCOs, and proteins sequences were used. These MCOs protein sequences were extracted from by doing fet3 protein sequence BLAST with wheat, *Arabidopsis* and *O. sativa* whole genome. In total 77 genes of *Triticum aestivum*, 12 of *Arabidopsis thaliana* and 12 of *Oryza sativa* were extracted from Plant ensemble. The putative IDs and protein sequences were then aligned using the MUSCLE algorithm (Edgar, 2004) and a rooted tree was constructed using the maximum likelihood method using MEGAX software (Kumar *et al.*, 2018). The phylogenetic tree was constructed to depict wheat, *Arabidopsis* and *O. sativa* MCOs which have the most similarity with yeast *fet3*. Twenty-nine high-confidence TaMCO proteins were divided into six clades on the basis of their sequence similarity. The gene structure for the TaMCO transcripts was then analysed to determine their conserved motif architecture. These conserved motifs were predicted using MEME (Bailey *et al.*, 2015). A total of 8 conserved motifs designated as motifs 1-8 were identified with varying lengths. Motifs 1,2,3,6 were conserved among yeast fet3 and TaMCOs. These motifs will be further subjected to more *in-silico* validation. Along with this, the arrangement of introns and exons of wheat MCOs and their homeologs analysed by using the Gene Structure Display Server (GSDS) (Hu *et al.*, 2014).

RNA extraction and gene expression analyses

Total RNA extractions were carried out using Trizol Reagent, following the protocol described by (Rio *et al.*, 2010). RNA quantity and purity were assessed using a NanoDrop™ Lite Spectrophotometer (ThermoFisher Scientific). To eliminate genomic DNA contamination, RNA samples underwent DNase treatment using TURBO™ DNase (Ambion,

Life Technologies). For qRT-PCR analysis, cDNA was synthesized from DNase-treated total RNA using the Invitrogen SuperScript III First-Strand Synthesis System SuperMix (ThermoFisher Scientific). Gene expression quantification was performed with the QuantiTect SYBR Green RT-PCR Kit (Qiagen, Germany) on a Bio-Rad CFX96 Real-Time PCR detection system. Gene-specific primers, designed to amplify a 150-250 bp region from all three homologs of the wheat genes, were generated using Oligocalc software. Primer sequences used in qRT-PCR are listed in **Table S6**. Relative transcript levels were calculated using the $2^{-\Delta\Delta CT}$ method (Livak and Schmittgen, 2001), with the ADP-ribosylation factor gene (TaARF) serving as an internal control.

Sub-cellular localization of TaMCO3

TaMCO3-5A (highly expressing) amplification was performed from pJET1.2 using gene-specific primers and subsequently ligated into the pENTR™/D-TOPO™ vector. Following sequence confirmation, an LR reaction was conducted with the positive TaMCO-pENTR TOPO and the pSITE-cEYFP vector. The resulting TaMCO3-cEYFP construct, along with the pSITE-cEYFP empty vector and the plasma membrane marker clone pMRK-RFP, was transformed into Agrobacterium strain GV3101. The transformed GV3101 cells were resuspended in an agroinfiltration medium [10 mM MES (pH 5.6), 10 mM MgCl2, and 200 µM acetosyringone] and used to inoculate the abaxial surfaces of six- to eight-week-old *Nicotiana benthamiana* leaves at an OD600 of 0.6-0.8 using syringe infiltration. The leaf tissues were visualized for fluorescent signals 48 hours post-infiltration using a LEICA DM600CS confocal microscope. YFP fluorescence was detected at 500–530 nm, and red fluorescence (RFP) was detected at 580–630 nm.

Wheat transformation, screening and immunolocalization of TaMCO3

To generate *TaMCO3* (B homoeologue) overexpression lines in the wheat variety 'Fielder,' Agrobacterium-mediated transformation was conducted according to the method described by (Hayta *et al.*, 2021). The construct *TaMCO3* in the pGWB520 vector was introduced into *Agrobacterium* strain AGL-1, and positive colonies were selected. Immature wheat embryos were transformed with the construct, where the *TaMCO3* cDNA was driven by the constitutive CaMV35S promoter. Transformed calli were selected on hygromycin at 50 mg/L for the first round of selection, 30 mg/L for the second, and 15 mg/L during the regeneration phase. The presence of the transgene in the regenerated plants was confirmed through PCR analysis (Hygromycin/M13 Primers), following the protocol of (Bhati *et al.*, 2016).

For whole-mount immunolocalization and confocal microscopy wheat root samples were fixed in methanol for 20 min. at 37°C. Immunolocalizations of sectioned wheat root were performed essentially as described earlier (Pasternak *et al.*, 2015). The primary antibody (anti-c-Myc tag monoclonal antibody Catalog no. M1001050; Thermofisher, USA) was diluted 1:100 in Blocking buffer (containing 2% bovine serum albumin in 1xMTSB buffer), and the secondary antibody (Alexa Flour™ Plus 488 anti-mouse Catalog no. A32723; Thermofisher, USA) was diluted 1:800 in blocking buffer. Antibody-treated sections were transferred to microscopic slides and observed with the confocal microscope. Images were captured in replicates at 10X using an Zeiss LSM 880 Confocal Laser Scanning Microscope.

Ferroxidase assay in wheat roots

To carry our ferroxidase assay seeds of *Triticum aestivum* cv. C306 were grown in control and iron-deficient media for 8 days and 14 days, from which total protein was isolated from roots by using HEPES buffer and PMSF, and the protein concentration was then quantified by using Bradford reagent protein estimation. An equal amount of protein was taken to perform the ferroxidase assay further. The oxidation of Fe (II) was assayed by monitoring the

rate of disappearance of ferrous ammonium sulfate using the ferrous chelator ferrozine. Reactions were carried out in microcentrifuge tubes containing 1050 µl buffer (450 mM Na-acetate (pH 5.8), 100 µl $CuSO_4$) and 15 µl of total protein from roots (2µg/ml). After which the reaction was initiated by adding 225 µl substrate ($Fe(II)SO_4$, 357 µM) containing 100 µM $CuSO_4$ (Müller *et al.*, 2015a). The aliquots (200µl) were then removed at appropriate intervals and transferred to 96 well microtiter plates for reaction-quenching with 14µl of 18mM ferrozine. The rate of Fe^{2+} oxidation for the Fe^{2+}-ferrozine complex was calculated from the decreased absorbance at 560nm and the graph was plotted (Hoopes and Dean, 2004b).

Acknowledgements

The authors thank the Executive Director for the facilities and support. This work was supported by the NABI-CORE grant to AKP. DBT-eLibrary Consortium (DeLCON) is acknowledged for providing timely support and access to e-resources for this work.

Contributions

Conceptualization: AKP, TL, SS and RJ; Project administration: AKP, JK; Investigation: RJ, DT, GS, VS; Formal analyses: RJ, VS, ER, VM, DT, GS, HB; Visualization: KA, VM, TL, Resources: SS, TL Methodology: All authors. Software: GS, VM, RJ; Validation: RJ, GS, DT, KA. Supervision: AKP, TL, SS, ER. Writing- Original draft: RJ, AKP, GS, KA; Writing- Review and Editing: TL, ER, SS, RJ; Funding Acquisition: AKP, TL.

Conflict of interest

The authors declare that they have no known competing financial interests or personal relationships that could have appeared to influence the work reported in this manuscript.

Data Availability

No datasets were generated or analysed during the current study.

References:

Ai, H., Cao, Y., Jain, A., et al. (2020) The ferroxidase LPR5 functions in the maintenance of phosphate homeostasis and is required for normal growth and development of rice. *J Exp Bot*, **71**, 4828–4843.

Bailey, T.L., Johnson, J., Grant, C.E. and Noble, W.S. (2015) The MEME Suite. *Nucleic Acids Res*, **43**, W39–W49. Available at: https://dx.doi.org/10.1093/nar/gkv416 [Accessed November 14, 2024].

Baluška, F., Kubica, S. and Hauskrecht, M. (1990) Postmitotic "isodiametric" cell growth in the maize root apex. *Planta*, **181**, 269–274. Available at: https://pubmed.ncbi.nlm.nih.gov/24196802/ [Accessed October 18, 2024].

Bernal, M. and Krämer, U. (2021) Involvement of Arabidopsis Multi-Copper Oxidase-Encoding LACCASE12 in Root-to-Shoot Iron Partitioning: A Novel Example of Copper-Iron Crosstalk. *Front Plant Sci*, **12**.

Bhati, K.K., Alok, A., Kumar, A., Kaur, J., Tiwari, S. and Pandey, A.K. (2016) Silencing of ABCC13 transporter in wheat reveals its involvement in grain development, phytic acid accumulation and lateral root formation. *J Exp Bot*, **67**, 4379–4389. Available at: https://dx.doi.org/10.1093/jxb/erw224 [Accessed October 18, 2024].

Brun, A., Smokvarska, M., Wei, L., Chay, S., Curie, C. and Mari, S. (2022) MCO1 and MCO3, two putative ascorbate oxidases with ferroxidase activity, new candidates for the regulation of apoplastic iron excess in Arabidopsis. *Plant Direct*, **6**, e463. Available at: https://onlinelibrary.wiley.com/doi/full/10.1002/pld3.463 [Accessed October 3, 2023].

Chen, C., Chen, H., Zhang, Y., Thomas, H.R., Frank, M.H., He, Y. and Xia, R. (2020) TBtools: An Integrative Toolkit Developed for Interactive Analyses of Big Biological Data. *Mol Plant*, **13**, 1194–1202.

Chen, W.W., Zhu, H.H., Wang, J.Y., Han, G.H., Huang, R.N., Hong, Y.G. and Yang, J.L. (2022) Comparative Physiological and Transcriptomic Analyses Reveal Altered Fe-Deficiency Responses in Tomato Epimutant Colorless Non-ripening. *Front Plant Sci*, **12**, 796893. Available at: https://pmc.ncbi.nlm.nih.gov/articles/PMC8813752/ [Accessed November 17, 2024].

Conte, S.S. and Walker, E.L. (2011) Transporters Contributing to Iron Trafficking in Plants. *Mol Plant*, **4**, 464–476. Available at: [Accessed November 17, 2024].

Curie, C., Cassin, G., Couch, D., et al. (2009) Metal movement within the plant: Contribution of nicotianamine and yellow stripe 1-like transporters. *Ann Bot*, **103**, 1–11.

Dinneny, J.R., Long, T.A., Wang, J.Y., et al. (2008) Cell identity mediates the response of Arabidopsis roots to abiotic stress. *Science*, **320**, 942–945. Available at: https://pubmed.ncbi.nlm.nih.gov/18436742/ [Accessed October 21, 2024].

Edgar, R.C. (2004) MUSCLE: A multiple sequence alignment method with reduced time and space complexity. *BMC Bioinformatics*, **5**, 1–19. Available at: https://bmcbioinformatics.biomedcentral.com/articles/10.1186/1471-2105-5-113 [Accessed November 14, 2024].

Gabay, G., Wang, H., Zhang, J., et al. (2023a) Dosage differences in 12-OXOPHYTODIENOATE REDUCTASE genes modulate wheat root growth. *Nature Communications 2023 14:1*, **14**, 1–15. Available at: https://www.nature.com/articles/s41467-023-36248-y [Accessed November 17, 2024].

Gabay, G., Wang, H., Zhang, J., et al. (2023b) Dosage differences in 12-OXOPHYTODIENOATE REDUCTASE genes modulate wheat root growth. *Nature Communications 2023 14:1*, **14**, 1–15. Available at: https://www.nature.com/articles/s41467-023-36248-y [Accessed October 21, 2024].

Gouran, M. and Brady, S.M. (2024) The transcriptional integration of environmental cues with root cell type development. *Plant Physiol*, **00**, 1–12. Available at: https://dx.doi.org/10.1093/plphys/kiae425 [Accessed October 21, 2024].

Gu, Y., Fu, C., Zhang, M., et al. (2024) Effects of OsLPR2 Gene Knockout on Rice Growth, Development, and Salt Stress Tolerance. *Agriculture (Switzerland)*, **14**, 1827. Available at: https://www.mdpi.com/2077-0472/14/10/1827/htm [Accessed November 14, 2024].

Hayta, S., Smedley, M.A., Clarke, M., Forner, M. and Harwood, W.A. (2021) An Efficient Agrobacterium-Mediated Transformation Protocol for Hexaploid and Tetraploid Wheat. *Curr Protoc*, **1**, e58. Available at: https://onlinelibrary.wiley.com/doi/full/10.1002/cpz1.58 [Accessed October 18, 2024].

Hoopes, J.T. and Dean, J.F.D. (2004a) Ferroxidase activity in a laccase-like multicopper oxidase from Liriodendron tulipifera. *Plant Physiology and Biochemistry*, **42**, 27–33.

Hoopes, J.T. and Dean, J.F.D. (2004b) Ferroxidase activity in a laccase-like multicopper oxidase from Liriodendron tulipifera. *Plant Physiology and Biochemistry*, **42**, 27–33.

Hu, B., Jin, J., Guo, A.Y., Zhang, H., Luo, J. and Gao, G. (2014) GSDS 2.0: an upgraded gene feature visualization server. *Bioinformatics*, **31**, 1296. Available at: https://pmc.ncbi.nlm.nih.gov/articles/PMC4393523/ [Accessed November 14, 2024].

Jiang, K., Moe-Lange, J., Hennet, L. and Feldman, L.J. (2016) Salt stress affects the redox status of arabidopsis root meristems. *Front Plant Sci*, **7**, 174867. Available at: www.frontiersin.org [Accessed October 18, 2024].

Kajala, K., Gouran, M., Shaar-Moshe, L., et al. (2021) Innovation, conservation, and repurposing of gene function in root cell type development. *Cell*, **184**, 3333-3348.e19. Available at: [Accessed October 21, 2024].

Kaur, G., Meena, V., Kumar, A., Suman, G., Tyagi, D., Joon, R., Balk, J. and Pandey, A.K. (2023) Asymmetric expression of homoeologous genes in wheat roots modulates the early phase of iron-deficiency signalling. *Environ Exp Bot*, **208**.

Kaur, G., Shukla, V., Kumar, A., et al. (2019) Integrative analysis of hexaploid wheat roots identifies signature components during iron starvation. *J Exp Bot*, **70**, 6141–6161.

Kobayashi, T., Nakanishi, H. and Nishizawa, N.K. (2010) Recent insights into iron homeostasis and their application in graminaceous crops. *Proc Jpn Acad Ser B Phys Biol Sci*, **86**, 900–913.

Kobayashi, T., Nakanishi Itai, R. and Nishizawa, N.K. (2014) Iron deficiency responses in rice roots. *Rice*, **7**, 1–11. Available at: https://thericejournal.springeropen.com/articles/10.1186/s12284-014-0027-0 [Accessed October 21, 2024].

Kobayashi, T. and Nishizawa, N.K. (2012) Iron uptake, translocation, and regulation in higher plants. *Annu Rev Plant Biol*, **63**, 131–152.

Kumar, S., Stecher, G., Li, M., Knyaz, C. and Tamura, K. (2018) MEGA X: Molecular Evolutionary Genetics Analysis across Computing Platforms. *Mol Biol Evol*, **35**, 1547–1549. Available at: https://pubmed.ncbi.nlm.nih.gov/29722887/ [Accessed November 14, 2024].

Li, G., Kronzucker, H.J. and Shi, W. (2016a) Root developmental adaptation to Fe toxicity: Mechanisms and management. *Plant Signal Behav*, **11**. Available at: https://pubmed.ncbi.nlm.nih.gov/26619064/ [Accessed October 21, 2024].

Li, G., Kronzucker, H.J. and Shi, W. (2016b) The Response of the Root Apex in Plant Adaptation to Iron Heterogeneity in Soil. *Front Plant Sci*, **7**, 344. Available at: https://pmc.ncbi.nlm.nih.gov/articles/PMC4800179/ [Accessed November 17, 2024].

Li, G., Kronzucker, H.J. and Shi, W. (2016c) The response of the root apex in plant adaptation to iron heterogeneity in soil. *Front Plant Sci*, **7**, 181664. Available at: www.frontiersin.org [Accessed October 21, 2024].

Li, M., Watanabe, S., Gao, F. and Dubos, C. (2023) Iron Nutrition in Plants: Towards a New Paradigm? *Plants 2023, Vol. 12, Page 384*, **12**, 384. Available at: https://www.mdpi.com/2223-7747/12/2/384/htm [Accessed November 8, 2024].

Liu, Q., Liang, Z., Feng, D., et al. (2021) Transcriptional landscape of rice roots at the single-cell resolution. *Mol Plant*, **14**, 384–394. Available at: https://pubmed.ncbi.nlm.nih.gov/33352304/ [Accessed October 21, 2024].

Liu, X.X., Zhang, H.H., Zhu, Q.Y., et al. (2022) Phloem iron remodels root development in response to ammonium as the major nitrogen source. *Nature Communications 2022 13:1*, **13**, 1–16. Available at: https://www.nature.com/articles/s41467-022-28261-4 [Accessed October 21, 2024].

Livak, K.J. and Schmittgen, T.D. (2001) Analysis of relative gene expression data using real-time quantitative PCR and the 2(-Delta Delta C(T)) Method. *Methods*, **25**, 402–408. Available at: https://pubmed.ncbi.nlm.nih.gov/11846609/ [Accessed November 18, 2024].

Martín-Barranco, A., Spielmann, J., Dubeaux, G., Vert, G. and Zelazny, E. (2020) Dynamic Control of the High-Affinity Iron Uptake Complex in Root Epidermal Cells. *Plant Physiol*, **184**, 1236–1250. Available at: https://dx.doi.org/10.1104/pp.20.00234 [Accessed November 17, 2024].

Meena, V., Kaur, G., Joon, R., Shukla, V., Choudhary, P., Roy, J.K., Singh, B. and Pandey, A.K. (2024) Transcriptome and biochemical analysis in hexaploid wheat with contrasting tolerance to iron deficiency pinpoints multi-layered molecular process. *Plant Physiology and Biochemistry*, **207**.

Molnár, Z., Solomon, W., Mutum, L. and Janda, T. (2023) Understanding the Mechanisms of Fe Deficiency in the Rhizosphere to Promote Plant Resilience. *Plants 2023, Vol. 12, Page 1945*, **12**, 1945. Available at: https://www.mdpi.com/2223-7747/12/10/1945/htm [Accessed November 17, 2024].

Morrissey, J., Baxter, I.R., Lee, J., Li, L., Lahner, B., Grotz, N., Kaplan, J., Salt, D.E. and Guerinot, M. Lou (2009) The ferroportin metal efflux proteins function in iron and cobalt homeostasis in Arabidopsis. *Plant Cell*, **21**, 3326–3338.

Müller, J., Toev, T., Heisters, M., Teller, J., Moore, K.L., Hause, G., Dinesh, D.C., Bürstenbinder, K. and Abel, S. (2015a) Iron-Dependent Callose Deposition Adjusts Root Meristem Maintenance to Phosphate Availability. *Dev Cell*, **33**, 216–230.

Müller, J., Toev, T., Heisters, M., Teller, J., Moore, K.L., Hause, G., Dinesh, D.C., Bürstenbinder, K. and Abel, S. (2015b) Iron-Dependent Callose Deposition Adjusts Root Meristem Maintenance to Phosphate Availability. *Dev Cell*, **33**, 216–230.

Naumann, C., Heisters, M., Brandt, W., et al. (2022) Bacterial-type ferroxidase tunes iron-dependent phosphate sensing during Arabidopsis root development. *Current Biology*, **32**, 2189-2205.e6.

Pasternak, T., Tietz, O., Rapp, K., Begheldo, M., Nitschke, R., Ruperti, B. and Palme, K. (2015) Protocol: An improved and universal procedure for whole-mount immunolocalization in plants. *Plant Methods*, **11**, 1–10. Available at:

https://plantmethods.biomedcentral.com/articles/10.1186/s13007-015-0094-2 [Accessed October 21, 2024].

Ramírez-González, R.H., Borrill, P., Lang, D., et al. (2018) The transcriptional landscape of polyploid wheat. *Science (1979)*, **361**. Available at: https://www.science.org/doi/10.1126/science.aar6089 [Accessed November 14, 2024].

Rio, D.C., Ares, M., Hannon, G.J. and Nilsen, T.W. (2010) Purification of RNA using TRIzol (TRI reagent). *Cold Spring Harb Protoc*, **2010**. Available at: https://pubmed.ncbi.nlm.nih.gov/20516177/ [Accessed November 18, 2024].

Robe, K. and Barberon, M. (2023) Nutrient carriers at the heart of plant nutrition and sensing. *Curr Opin Plant Biol*, **74**, 102376. Available at: [Accessed November 8, 2024].

Santi, S. and Schmidt, W. (2009) Dissecting iron deficiency-induced proton extrusion in Arabidopsis roots. *New Phytologist*, **183**, 1072–1084.

Schaaf, G., Schikora, A., Häberle, J., Vert, G., Ludewig, U., Briat, J.F., Curie, C. and Wirén, N. Von (2005) A Putative Function for the Arabidopsis Fe–Phytosiderophore Transporter Homolog AtYSL2 in Fe and Zn Homeostasis. *Plant Cell Physiol*, **46**, 762–774. Available at: https://dx.doi.org/10.1093/pcp/pci081 [Accessed October 21, 2024].

Shahan, R., Hsu, C.W., Nolan, T.M., et al. (2022) A single-cell Arabidopsis root atlas reveals developmental trajectories in wild-type and cell identity mutants. *Dev Cell*, **57**, 543-560.e9. Available at: https://pubmed.ncbi.nlm.nih.gov/35134336/ [Accessed October 21, 2024].

Silva, D.M. De, Askwith, C.C., Eide, D. and Kaplan, J. (1995) The FET3 gene product required for high affinity iron transport in yeast is a cell surface ferroxidase. *Journal of Biological Chemistry*, **270**, 1098–1101.

Stoj, C. and Kosman, D.J. (2003) Cuprous oxidase activity of yeast Fet3p and human ceruloplasmin: implication for function. *FEBS Lett*, **554**, 422–426. Available at: [Accessed November 17, 2024].

Sun, H., Feng, F., Liu, J. and Zhao, Q. (2017) The interaction between auxin and nitric oxide regulates root growth in response to iron deficiency in rice. *Front Plant Sci*, **8**, 317201. Available at: [Accessed November 17, 2024].

Tian, T., Liu, Y., Yan, H., You, Q., Yi, X., Du, Z., Xu, W. and Su, Z. (2017) AgriGO v2.0: A GO analysis toolkit for the agricultural community, 2017 update. *Nucleic Acids Res*, **45**, W122–W129.

Turlapati, P. V., Kim, K.W., Davin, L.B. and Lewis, N.G. (2011) The laccase multigene family in Arabidopsis thaliana: Towards addressing the mystery of their gene function(s). *Planta*, **233**, 439–470. Available at: https://link.springer.com/article/10.1007/s00425-010-1298-3 [Accessed October 21, 2024].

Vashchenko, G. and MacGillivray, R.T.A. (2013) Multi-copper oxidases and human iron metabolism. *Nutrients*, **5**, 2289–2313.

Wang, M., Kawakami, Y. and Bhullar, N.K. (2019) Molecular Analysis of Iron Deficiency Response in Hexaploid Wheat. *Front Sustain Food Syst*, **3**, 1–14.

Wang, Y., Kang, Y., Zhong, M., Zhang, L., Chai, X., Jiang, X. and Yang, X. (2022) Effects of Iron Deficiency Stress on Plant Growth and Quality in Flowering Chinese Cabbage and Its Adaptive Response. *Agronomy 2022, Vol. 12, Page 875*, **12**, 875. Available at: https://www.mdpi.com/2073-4395/12/4/875/htm [Accessed November 17, 2024].

Xu, Z.R., Cai, M.L., Yang, Y., You, T.T., Ma, J.F., Wang, P. and Zhao, F.J. (2022) The ferroxidases LPR1 and LPR2 control iron translocation in the xylem of Arabidopsis plants. *Mol Plant*, **15**, 1962–1975.

Yi, Y. and Guerinot, M. Lou (1996) Genetic evidence that induction of root Fe(III) chelate reductase activity is necessary for iron uptake under iron deficiency. *Plant J*, **10**, 835–844. Available at: https://pubmed.ncbi.nlm.nih.gov/8953245/ [Accessed October 18, 2024].

Yokosho, K., Yamaji, N., Ueno, D., Mitani, N. and Jian, F.M. (2009) OsFRDL1 Is a Citrate Transporter Required for Efficient Translocation of Iron in Rice. *Plant Physiol*, **149**, 297. Available at: https://pmc.ncbi.nlm.nih.gov/articles/PMC2613705/ [Accessed November 17, 2024].

Zanin, L., Venuti, S., Zamboni, A., Varanini, Z., Tomasi, N. and Pinton, R. (2017) Transcriptional and physiological analyses of Fe deficiency response in maize reveal the presence of Strategy I components and Fe/P interactions. *BMC Genomics*, **18**, 1–15. Available at: https://bmcgenomics.biomedcentral.com/articles/10.1186/s12864-016-3478-4 [Accessed November 17, 2024].

Zhang, L., He, C., Lai, Y., et al. (2023a) Asymmetric gene expression and cell-type-specific regulatory networks in the root of bread wheat revealed by single-cell multiomics analysis. *Genome Biology 2023 24:1*, **24**, 1–25. Available at: https://genomebiology.biomedcentral.com/articles/10.1186/s13059-023-02908-x [Accessed October 21, 2024].

Zhang, L., He, C., Lai, Y., et al. (2023b) Asymmetric gene expression and cell-type-specific regulatory networks in the root of bread wheat revealed by single-cell multiomics analysis. *Genome Biology 2023 24:1*, **24**, 1–25. Available at: https://genomebiology.biomedcentral.com/articles/10.1186/s13059-023-02908-x [Accessed November 18, 2024].

Zhang, L., Li, G., Wang, M., Di, D., Sun, L., Kronzucker, H.J. and Shi, W. (2018) Excess iron stress reduces root tip zone growth through nitric oxide-mediated repression of potassium homeostasis in Arabidopsis. *New Phytologist*, **219**, 259–274. Available at: https://onlinelibrary.wiley.com/doi/full/10.1111/nph.15157 [Accessed October 18, 2024].

Zhang, T.Q., Chen, Y., Liu, Y., Lin, W.H. and Wang, J.W. (2021) Single-cell transcriptome atlas and chromatin accessibility landscape reveal differentiation trajectories in the rice root. *Nat Commun*, **12**. Available at: https://pubmed.ncbi.nlm.nih.gov/33824350/ [Accessed October 21, 2024].

Zhang, T.Q., Xu, Z.G., Shang, G.D. and Wang, J.W. (2019) A Single-Cell RNA Sequencing Profiles the Developmental Landscape of Arabidopsis Root. *Mol Plant*, **12**, 648–660. Available at: https://pubmed.ncbi.nlm.nih.gov/31004836/ [Accessed October 21, 2024].

Zhang, Y., Wang, Y.P., Liu, P., Song, J.M., Xu, G.D. and Zheng, G.H. (2012) Effect of toxic Fe 2+ levels on the biological characteristics of rice root border cells. *Russian Journal of Plant Physiology*, **59**, 766–771. Available at: https://link.springer.com/article/10.1134/S1021443712060209 [Accessed October 21, 2024].

Zhang, Y., Zheng, G.H., Liu, P., Song, J.M., Xu, G. Di and Cai, M.Z. (2011) Morphological and physiological responses of root tip cells to Fe2+ toxicity in rice. *Acta Physiol Plant*, **3**, 683–689. Available at: https://www.infona.pl//resource/bwmeta1.element.springer-d5936b60-d7a5-3ba7-b08b-f7446cd88022 [Accessed October 21, 2024].

Zhao, J., Meng, X., Zhang, Z., Wang, M., Nie, F. and Liu, Q. (2023) OsLPR5 Encoding Ferroxidase Positively Regulates the Tolerance to Salt Stress in Rice. *Int J Mol Sci*, **24**, 8115. Available at: https://pmc.ncbi.nlm.nih.gov/articles/PMC10179522/ [Accessed October 21, 2024].

Zheng, Y., Jiao, C., Sun, H., et al. (2016) iTAK: A Program for Genome-wide Prediction and Classification of Plant Transcription Factors, Transcriptional Regulators, and Protein Kinases. *Mol Plant*, **9**, 1667–1670.

Zhu, Q.Y., Wang, Y., Liu, X.X., et al. (2022a) The ferroxidases are critical for Fe(II) oxidation in xylem to ensure a healthy Fe allocation in Arabidopsis thaliana. *Front Plant Sci*, **13**.

Zhu, Q.Y., Wang, Y., Liu, X.X., et al. (2022b) The ferroxidases are critical for Fe(II) oxidation in xylem to ensure a healthy Fe allocation in Arabidopsis thaliana. *Front Plant Sci*, **13**, 958984. Available at: https://pmc.ncbi.nlm.nih.gov/articles/PMC9428407/ [Accessed October 21, 2024].

Legends for the Figures:

Figure 1: Analysis of the RNAseq from the wheat root tip. **(A)** schematic representation of the wheat root tip highlights the three distinct root zones: maturation, elongation, and meristematic zones. Lower right, microscopy images of root tips under both +Fe (iron-sufficient) and –Fe (Fe deficiency) conditions (Perls/DAB staining), illustrating morphological differences in these zones. The region from which tissue was collected for subsequent RNA-seq analysis is marked on the diagram, corresponding to first 1-2.5mm of the root, which mostly includes the meristematic zone of the total root. **(B)** Volcano plot illustrating the differential gene expression between +Fe (iron-sufficient) and –Fe (Fe deficiency) root tip samples subjected to RNA-seq analysis. The plot highlights the statistical significance (y-axis, -log10 p-value) versus the magnitude of change (x-axis, log2 fold change) for each gene. Genes with significant upregulation under –Fe conditions are indicated on the right (red colour), while those downregulated are on the left. **(C)** Venn diagram showing the overlap of upregulated genes among three conditions: root tip –Fe treated samples, 4-day –Fe treated samples, and 8-day –Fe treated samples. The diagram identifies genes that are commonly upregulated across all conditions as well as those that are uniquely upregulated under each specific condition, highlighting both shared and condition-specific responses to iron deficiency in wheat.

Figure 2: Comparative GO annotation of the various DEGs expressed under –Fe. **(A)** Heatmap depicting the expression patterns of differentially expressed genes (DEGs) under –Fe (4 and 8 days) and root tip –Fe conditions. The color scale represents the relative expression levels across the different conditions, illustrating both the upregulation and downregulation of these genes in response to iron deficiency. **(B)** Gene Ontology (GO) enrichment analysis for –Fe DEGs for "root tip-specific" responses. For this a total of 5036 differentially expressed genes (DEGs) were analysed, revealing significant enrichment in biological processes related to metal ion transport and other cellular responses. **(C)** Gene Ontology (GO) enrichment analysis for 567 common differentially expressed genes (DEGs) identified in both root tip (–Fe 8D) and whole root samples (–Fe 8D) under –Fe conditions.

Figure 3: GO enrichment of the sub-genome transcripts and identification of –Fe induced wheat MCOs. **(A)** GO enrichment analysis was conducted for wheat homeologue-specific gene expression, revealing various pathways involved in the A, B, and D genomes of hexaploid wheat. The analysis highlights the distinct pathways associated with gene expression across the different wheat genomes, providing insights into the functional roles of these homeologous genes. **(B)** GO enrichment analysis and heat maps of multiple MCOs in wheat root tip showing differential expression in –Fe conditions. The analysis illustrates the significance of oxidoreductase activity in the regulation of iron in wheat. Heat map of the multi-copper oxidase (MCO) family, constructed based on RNA-seq data from wheat roots at 4 days and 8 days of –Fe (Kaur *et al*., 2023). The heat map on the left side indicates the expression levels of different wheat MCO genes across these conditions, highlighting their dynamic regulation in response to changes in rhizospheric Fe.

Figure 4: Expression and phylogenetic analysis of differentially expressed wheat MCOs. **(A)** A phylogenetic tree of Fet3-like genes was constructed, including ScFET3 (NP_013774), Uma Fer1 (XP_011386068), EcoMCO (EDU66368), Ceruloplasmin (EAW78883), AtMCOs

(LAC1-17, LPR1-2, MCO1-3), and TaMCOs. MCO proteins were aligned using the MUSCLE algorithm, and an unrooted phylogenetic tree was generated using the neighbor-joining method with MEGA 11, incorporating a bootstrap value of 1000. **(B)** qRT-PCR analysis of *TaMCO* genes. Wheat seedlings subjected to different concentration of Fe-EDTA as +Fe (80 µM) and –Fe (1 µM) and resupply (80 µM) for 4 and 8 days under hydroponic conditions. Each bar indicates the mean of three replicates with the indicated standard deviation of the mean. C_t values were normalized using wheat ARF1 as an internal control.

Figure 5: Characterization of the wheat candidate ferroxidases**. (A)** Domain analysis showing that plasma membrane domain is missing in TaMCO, while the cupredoxin and ascorbate oxidase domains were found to be conserved. **(B)** Expression of *TaMCO3* under various Fe dosage. **(C)** Expression of *TaMCO3* under different pH conditions, The expression was normalized using *TaARF1* as internal control, and fold change was calculated using the $2^{-\Delta\Delta CT}$ method. Vertical bars indicate the standard deviation (n=3), and letters above the bars indicate significant differences ($P<0.05$) between the various tissues by one way ANOVA test. **(D)** A yeast complementation assay was performed with the yeast *fet3fet4*Δ mutant, which exhibited growth impairment compared to the wild-type BY4741. However, growth was partially restored upon the addition of TaMCO-PM. Fe(II) disappearance in yeast total protein was measured using ferrozine as the chelator. **(E)** Wheat MCOs were cloned pRS315TEF_GFP vector for localization studies in *Saccharomyces cerevisiae*. Images were acquired using LEICA DM600CS confocal microscope and processed with Fiji-ImageJ. GFP fluorescence was detected at 500– 530 nm, pRS315TEF_GFP empty vector, pRS315TEF_GFP:TaMCO3 with magnification 25x and 40x. **(F)** The graph depicts ferroxidase activity by plotting Fe(II) disappearance, with total protein isolated from yeast cells. The complemented strain TaMCO3 in *fet3fet4*Δ mutant shows higher Fe(II) disappearance, indicating increased ferroxidase activity, compared to the yeast mutant

(*fet3fet4*). In contrast, the wild-type strain (BY4741) demonstrates greater Fe^{2+} disappearance than the fet3fet4Δ mutant.

Figure 6: Localization studies of TaMCO3 and complementation of atmco3 with TaMCO3**.** **(A)** Wheat MCOs localization was studied in *Nicotiana benthamiana*. Images were acquired 48 hours post-agroinfiltration using a LEICA DM600CS confocal microscope and processed with Fiji-ImageJ. Red fluorescence was detected at 580–630 nm. The first panel shows the plasma membrane marker pMRK-RFP, then TaMCO3-YFP, and at last an overlay of TaMCO3-YFP with pMRK-RFP with magnifications of 25x. **(B)** An overexpression line of TaMCO3 was generated in an *atmco3* mutant background, demonstrating rescue of the Arabidopsis knockout mutant *atmco3* phenotype. Plants were grown on Hoagland solid medium for 5 days, then transferred to +Fe (300 µM FeEDTA) and –Fe (300 µM Ferrozine) media for 2 weeks. Under all conditions, the *atmco3* mutant exhibited stunted growth compared to Col-0 plants. However, Arabidopsis lines overexpressing TaMCO3 showed a reversal in the mutant phenotype, resulting in increased primary root growth. **(C)** The graph shows root lengths measured using ImageJ software (Version 1.38). The values presented are representative of seven independent biological replicates. Letters above the bars indicate significant differences ($P < 0.05$) between genotypes, as determined by a two-way ANOVA test. **(D)** Iron distribution analysis was performed on roots of Col-0, *atmco3*, and TaMCO3 overexpressing Arabidopsis lines. Arabidopsis seedlings were germinated on Hoagland agar media for 5 days and then transferred to Hoagland minimal media amended with +Fe (80 µM FeEDTA), −Fe (300 µM Ferrozine), and ++Fe (300 µM FeEDTA) for 10 days. Perls staining was conducted to visualize iron accumulation in the roots. Greater accumulation of iron was observed in Col-0 and TaMCO3 overexpression lines under +Fe conditions. **(E)** The data were further confirmed using ICP-MS. The graph displays mean iron content with error bars representing standard deviation. Different letters above the bars indicate statistically

significant differences ($P < 0.05$) between genotypes, as determined by one-way ANOVA. **(F)** Expression analysis of *AtIRT* and **(G)** *AtFRO2* in Col-0, *atmco3* and *TaMCO3* overexpressing lines.

Figure 7: Expression characterization of TaMCO3 and its overexpression in wheat. **(A)** *In-silico* expression analysis of *TaMCO3* in different tissues during the developmental time course of plant development. **(B)** Gene expression analysis of *TaMCO3* in different genetic background as reported by (Gabay *et al.*, 2023a). **(C)** Ferrozine and Perls staining on wheat root tip, grown in media supplemented with Fe_2SO□. The Ferrozine staining intensity decreases over time, indicating a reduction in Fe^{2+} ion concentration at the root tip and Perl staining increasing over time indicating more accumulation of Fe^{3+}. This observation suggests a dynamic process of Fe^{2+} oxidation or transport, leading to lower detectable levels of Fe^{2+} at the root tip as time progresses. **(D)** This graph depicts the Fe^{2+} concentration (in μM) measured after treating FeSO□ substrate with total root protein under control (80 μM Fe-EDTA) and –Fe (1 μM Fe-EDTA) conditions. The assay included three biological replicates and three technical replicates. The Fe^{2+}-ferrozine complex formation was measured at 560 nm absorbance. A decreased absorbance of the Fe^{2+}-ferrozine complex in the iron-starved samples indicates increased oxidation of Fe^{2+} in the media. **(E)** Whole-mount immunolocalization of leaf tissue was carried out for WT and *TaMCO3* overexpression line, antibody-treated sections were transferred to microscopic slides and observed with confocal microscope. Images were captured in replicates at 10X using an Zeiss LSM 880 Confocal Laser Scanning Microscope. **(F)** Phenotypic response of Wild type and *TaMCO3* overexpression line grown under control (+Fe) and –Fe conditions along with their respective SPAD value. **(G)** Total Iron content of root and shoot was measure using ICP-MS of both WT and TaMCO3 overexpression line under control (+Fe) and iron deficiency (–Fe) conditions.

Figure 8: Gene expression of the Fe responsive gene and model summary. **(A)** Expression analysis of Fe homeostasis downstream genes in *TaMCO3* overexpressing lines. **(B)** The model summarizing the key molecular and biochemical mechanisms uncovered in the study, highlighting the role of TaMCO3, a wheat multicopper oxidase, in mediating iron uptake and mobilization. The known TOM proteins assist in DMA efflux of a major PS in wheat. Once the Fe-Chelates (Fe-PS) complex are formed they are subsequently transported in the epidermis by TaYS1A and is traversed to different cell-types will it reaches to the pericycle region. At this point the iron in Fe^{2+} is oxidised by ferroxidases (MCO as identified here as TaMCO3) to Fe^{3+} that is complexed mostly with citrate/malate and is traversed to long distance Fe mobilization to the foliar parts.

Supplementary Tables

Table S1: DEGs in response to –Fe in root tip with respect to their control samples.

Table S2: GO enrichment result of DEGs 8-Day root tip subjected to –Fe.

Table S3: GO enrichment result of DEGs common between 8-Day total root vs root tip.

Table S4: GO enrichment analysis of wheat genome encoding from A/B/ D homoeologs DEGs.

Table S5: GO enrichment result of root tips DEGs for oxido-reductase/redox activity.

Table S6: List of primers used in the current study.

(A)

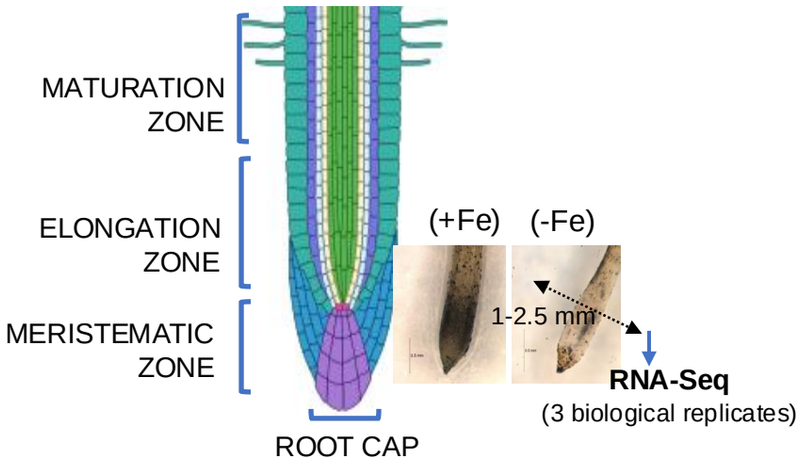
MATURATION ZONE
ELONGATION ZONE
MERISTEMATIC ZONE
ROOT CAP
(+Fe)
(-Fe)
1-2.5 mm
RNA-Seq
(3 biological replicates)

(B)

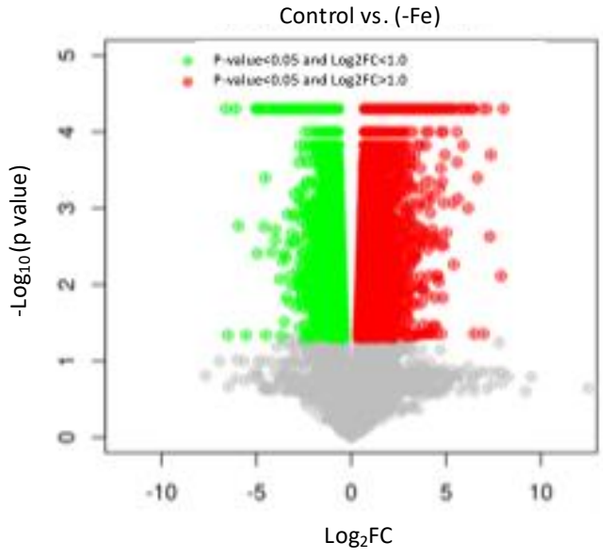
Control vs. (-Fe)
P-value<0.05 and Log2FC<1.0
P-value<0.05 and Log2FC>1.0
-Log10(p value)
Log2FC
-10
-5
0
5
10
0
1
2
3
4
5

(C)

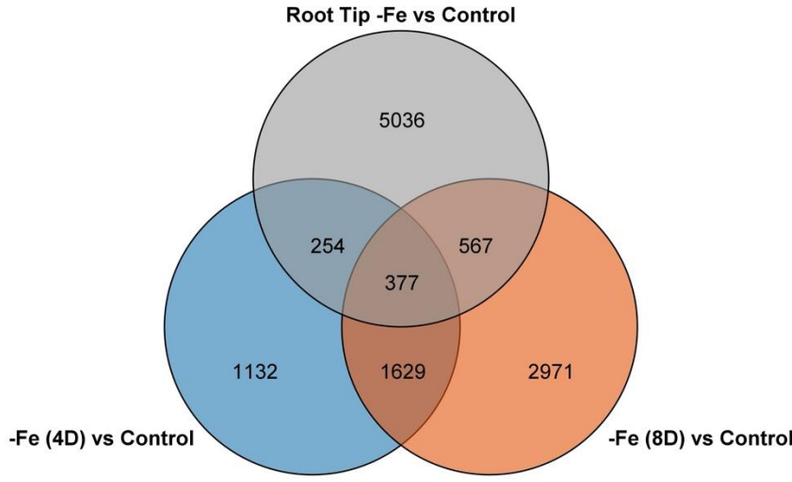
Root Tip -Fe vs Control
5036
254
567
377
1132
1629
2971
-Fe (4D) vs Control
-Fe (8D) vs Control

Figure 1

(A)

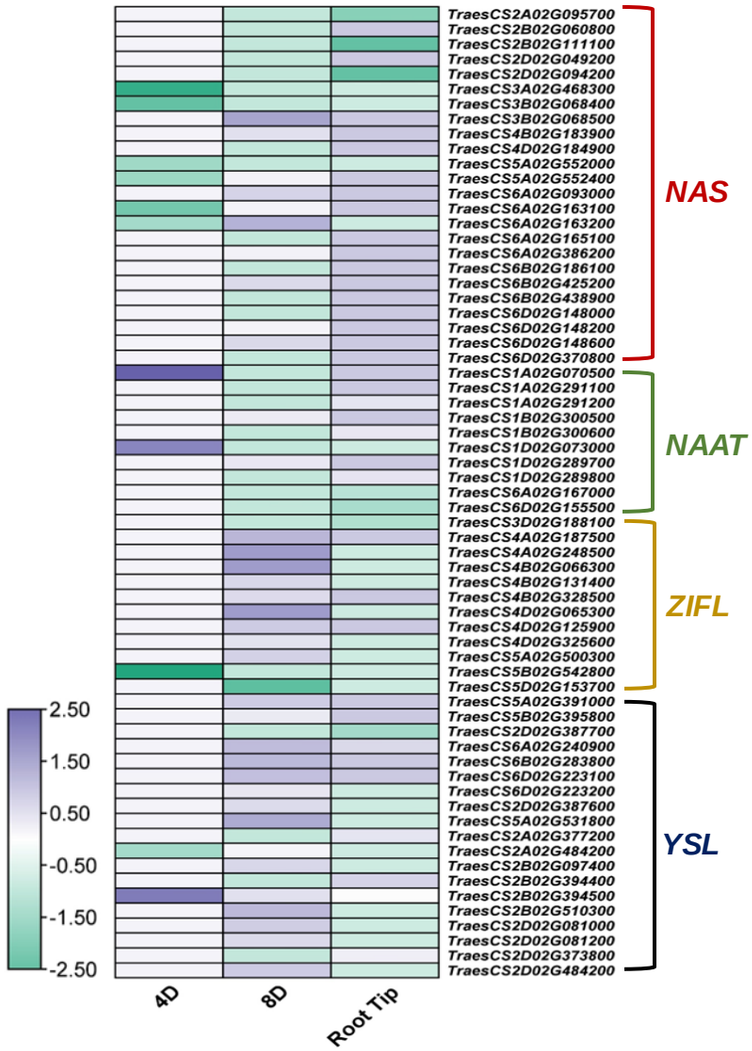
TraesCS2A02G095700
TraesCS2B02G060800
TraesCS2B02G111100
TraesCS2D02G049200
TraesCS2D02G094200
TraesCS3A02G468300
TraesCS3B02G068400
TraesCS3B02G068500
TraesCS4B02G183900
TraesCS4D02G184900
TraesCS5A02G552000
TraesCS5A02G552400
TraesCS6A02G093000
TraesCS6A02G163100
TraesCS6A02G163200
TraesCS6A02G165100
TraesCS6A02G386200
TraesCS6B02G186100
TraesCS6B02G425200
TraesCS6B02G438900
TraesCS6D02G148000
TraesCS6D02G148200
TraesCS6D02G148600
TraesCS6D02G370800
TraesCS1A02G070500
TraesCS1A02G291100
TraesCS1A02G291200
TraesCS1B02G300500
TraesCS1B02G300600
TraesCS1D02G073000
TraesCS1D02G289700
TraesCS1D02G289800
TraesCS6A02G167000
TraesCS6D02G155500
TraesCS3D02G188100
TraesCS4A02G187500
TraesCS4A02G248500
TraesCS4B02G066300
TraesCS4B02G131400
TraesCS4B02G328500
TraesCS4D02G065300
TraesCS4D02G125900
TraesCS4D02G325600
TraesCS5A02G500300
TraesCS5B02G542800
TraesCS5D02G153700
TraesCS5A02G391000
TraesCS5B02G395800
TraesCS2D02G387700
TraesCS6A02G240900
TraesCS6B02G283800
TraesCS6D02G223100
TraesCS6D02G223200
TraesCS2D02G387600
TraesCS5A02G531800
TraesCS2A02G377200
TraesCS2A02G484200
TraesCS2B02G097400
TraesCS2B02G394400
TraesCS2B02G394500
TraesCS2B02G510300
TraesCS2D02G081000
TraesCS2D02G081200
TraesCS2D02G373800
TraesCS2D02G484200
NAS
NAAT
ZIFL
YSL
2.50
1.50
0.50
-0.50
-1.50
-2.50
4D
8D
Root Tip

(B)

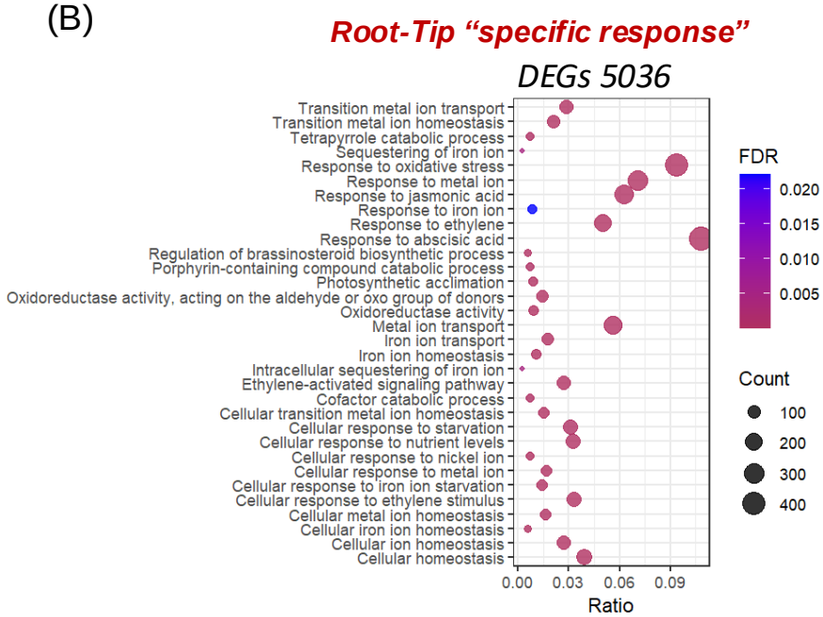
Root-Tip "specific response"
DEGs 5036
Transition metal ion transport
Transition metal ion homeostasis
Tetrapyrrole catabolic process
Sequestering of iron ion
Response to oxidative stress
Response to metal ion
Response to jasmonic acid
Response to iron ion
Response to ethylene
Response to abscisic acid
Regulation of brassinosteroid biosynthetic process
Porphyrin-containing compound catabolic process
Photosynthetic acclimation
Oxidoreductase activity, acting on the aldehyde or oxo group of donors
Oxidoreductase activity
Metal ion transport
Iron ion transport
Iron ion homeostasis
Intracellular sequestering of iron ion
Ethylene-activated signaling pathway
Cofactor catabolic process
Cellular transition metal ion homeostasis
Cellular response to starvation
Cellular response to nutrient levels
Cellular response to nickel ion
Cellular response to metal ion
Cellular response to iron ion starvation
Cellular response to ethylene stimulus
Cellular metal ion homeostasis
Cellular iron ion homeostasis
Cellular ion homeostasis
Cellular homeostasis
0.00
0.03
0.06
0.09
Ratio
FDR
0.020
0.015
0.010
0.005
Count
100
200
300
400

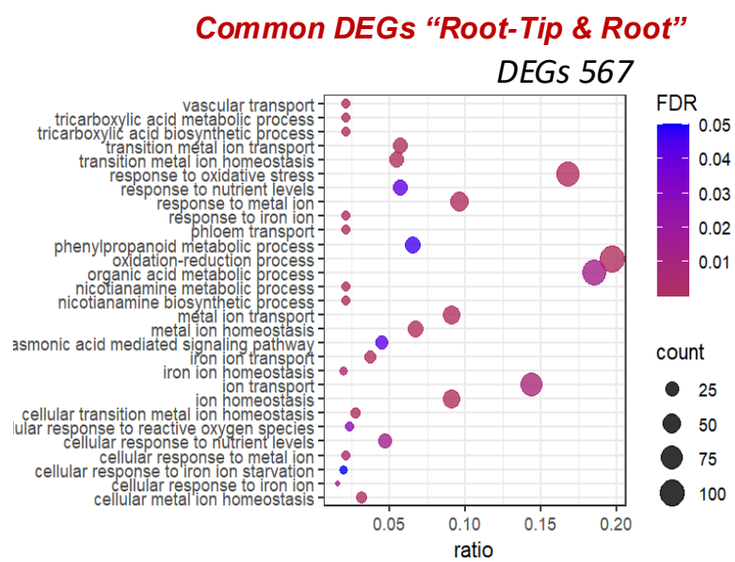
Common DEGs "Root-Tip & Root"
DEGs 567
vascular transport
tricarboxylic acid metabolic process
tricarboxylic acid biosynthetic process
transition metal ion transport
transition metal ion homeostasis
response to oxidative stress
response to nutrient levels
response to metal ion
response to iron ion
phloem transport
phenylpropanoid metabolic process
oxidation-reduction process
organic acid metabolic process
nicotianamine metabolic process
nicotianamine biosynthetic process
metal ion transport
metal ion homeostasis
asmonic acid mediated signaling pathway
iron ion transport
iron ion homeostasis
ion transport
ion homeostasis
cellular transition metal ion homeostasis
ular response to reactive oxygen species
cellular response to nutrient levels
cellular response to metal ion
cellular response to iron ion starvation
cellular response to iron ion
cellular metal ion homeostasis
0.05
0.10
0.15
0.20
ratio
FDR
0.05
0.04
0.03
0.02
0.01
count
25
50
75
100

Figure 2

(A)

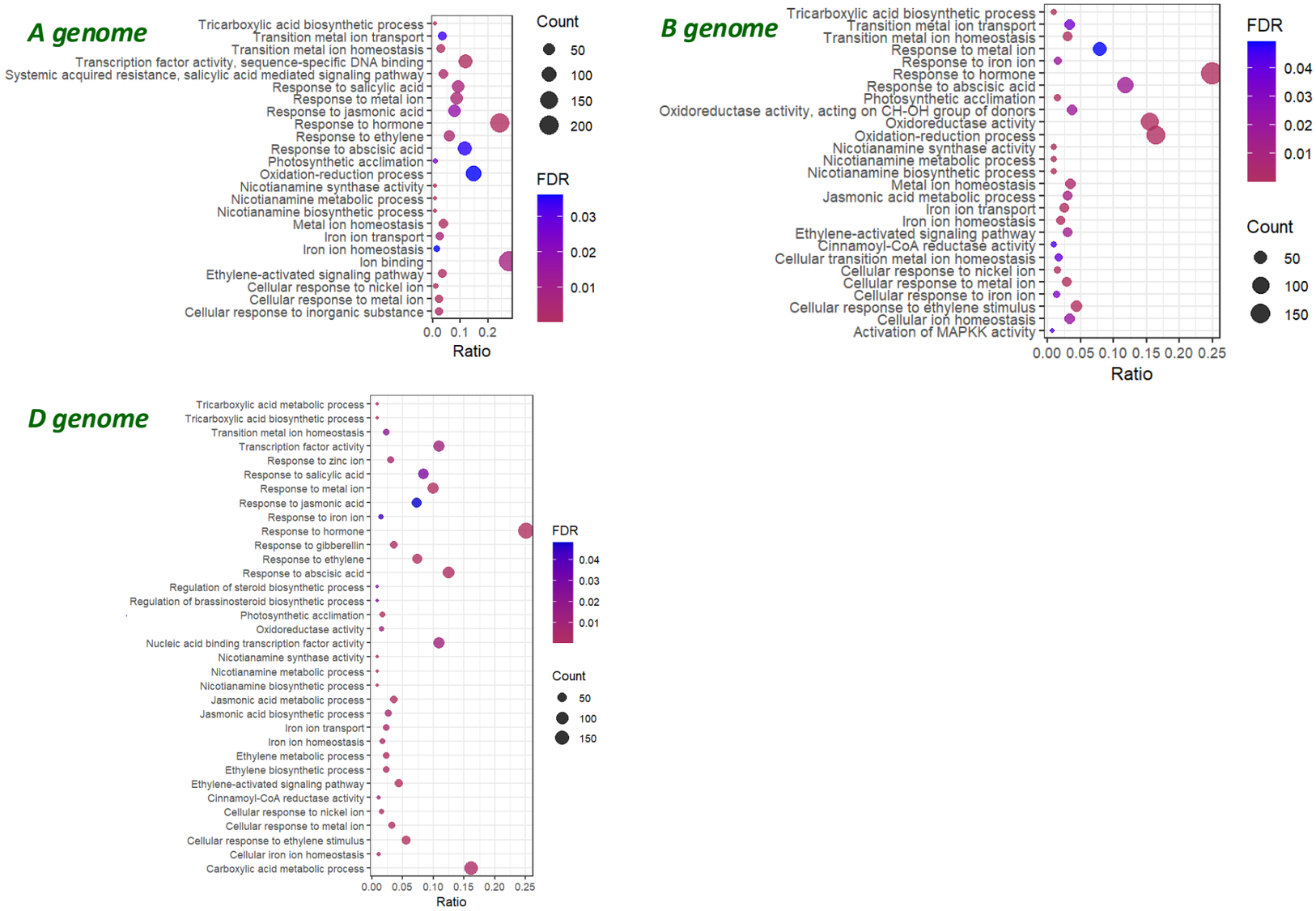
A genome
Tricarboxylic acid biosynthetic process
Transition metal ion transport
Transition metal ion homeostasis
Transcription factor activity, sequence-specific DNA binding
Systemic acquired resistance, salicylic acid mediated signaling pathway
Response to salicylic acid
Response to metal ion
Response to jasmonic acid
Response to hormone
Response to ethylene
Response to abscisic acid
Photosynthetic acclimation
Oxidation-reduction process
Nicotianamine synthase activity
Nicotianamine metabolic process
Nicotianamine biosynthetic process
Metal ion homeostasis
Iron ion transport
Iron ion homeostasis
Ion binding
Ethylene-activated signaling pathway
Cellular response to nickel ion
Cellular response to metal ion
Cellular response to inorganic substance
0.0 0.1 0.2
Ratio
Count
50
100
150
200
FDR
0.03
0.02
0.01
B genome
Tricarboxylic acid biosynthetic process
Transition metal ion transport
Transition metal ion homeostasis
Response to metal ion
Response to iron ion
Response to hormone
Response to abscisic acid
Photosynthetic acclimation
Oxidoreductase activity, acting on CH-OH group of donors
Oxidoreductase activity
Oxidation-reduction process
Nicotianamine synthase activity
Nicotianamine metabolic process
Nicotianamine biosynthetic process
Metal ion homeostasis
Jasmonic acid metabolic process
Iron ion transport
Iron ion homeostasis
Ethylene-activated signaling pathway
Cinnamoyl-CoA reductase activity
Cellular transition metal ion homeostasis
Cellular response to nickel ion
Cellular response to metal ion
Cellular response to iron ion
Cellular response to ethylene stimulus
Cellular ion homeostasis
Activation of MAPKK activity
0.00 0.05 0.10 0.15 0.20 0.25
Ratio
FDR
0.04
0.03
0.02
0.01
Count
50
100
150
D genome
Tricarboxylic acid metabolic process
Tricarboxylic acid biosynthetic process
Transition metal ion homeostasis
Transcription factor activity
Response to zinc ion
Response to salicylic acid
Response to metal ion
Response to jasmonic acid
Response to iron ion
Response to hormone
Response to gibberellin
Response to ethylene
Response to abscisic acid
Regulation of steroid biosynthetic process
Regulation of brassinosteroid biosynthetic process
Photosynthetic acclimation
Oxidoreductase activity
Nucleic acid binding transcription factor activity
Nicotianamine synthase activity
Nicotianamine metabolic process
Nicotianamine biosynthetic process
Jasmonic acid metabolic process
Jasmonic acid biosynthetic process
Iron ion transport
Iron ion homeostasis
Ethylene metabolic process
Ethylene biosynthetic process
Ethylene-activated signaling pathway
Cinnamoyl-CoA reductase activity
Cellular response to nickel ion
Cellular response to metal ion
Cellular response to ethylene stimulus
Cellular iron ion homeostasis
Carboxylic acid metabolic process
0.00 0.05 0.10 0.15 0.20 0.25
Ratio
FDR
0.04
0.03
0.02
0.01
Count
50
100
150

(B)

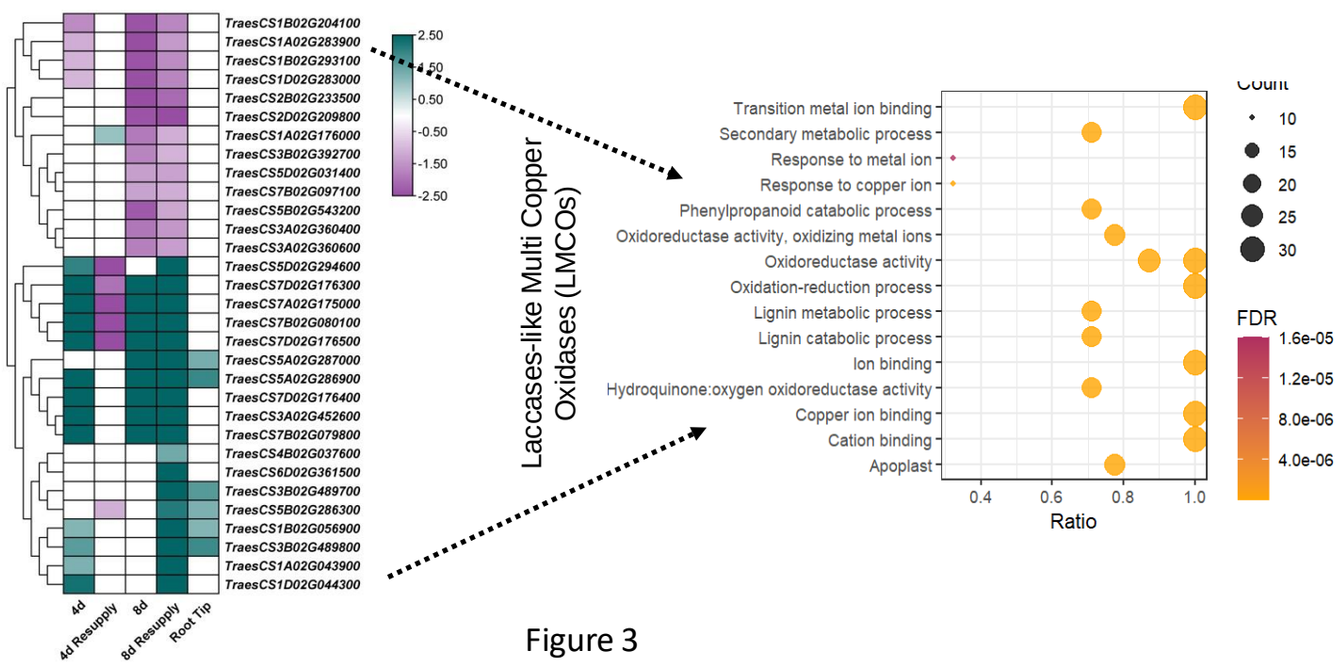
TraesCS1B02G204100
TraesCS1A02G283900
TraesCS1B02G293100
TraesCS1D02G283000
TraesCS2B02G233500
TraesCS2D02G209800
TraesCS1A02G176000
TraesCS3B02G392700
TraesCS5D02G031400
TraesCS7B02G097100
TraesCS5B02G543200
TraesCS3A02G360400
TraesCS3A02G360600
TraesCS5D02G294600
TraesCS7D02G176300
TraesCS7A02G175000
TraesCS7B02G080100
TraesCS7D02G176500
TraesCS5A02G287000
TraesCS5A02G286900
TraesCS7D02G176400
TraesCS3A02G452600
TraesCS7B02G079800
TraesCS4B02G037600
TraesCS6D02G361500
TraesCS3B02G489700
TraesCS5B02G286300
TraesCS1B02G056900
TraesCS3B02G489800
TraesCS1A02G043900
TraesCS1D02G044300
2.50
1.50
0.50
-0.50
-1.50
-2.50
4d
4d Resupply
8d
8d Resupply
Root Tip
Laccases-like Multi Copper Oxidases (LMCOs)
Transition metal ion binding
Secondary metabolic process
Response to metal ion
Response to copper ion
Phenylpropanoid catabolic process
Oxidoreductase activity, oxidizing metal ions
Oxidoreductase activity
Oxidation-reduction process
Lignin metabolic process
Lignin catabolic process
Ion binding
Hydroquinone:oxygen oxidoreductase activity
Copper ion binding
Cation binding
Apoplast
0.4 0.6 0.8 1.0
Ratio
Count
10
15
20
25
30
FDR
1.6e-05
1.2e-05
8.0e-06
4.0e-06

Figure 3

(A)

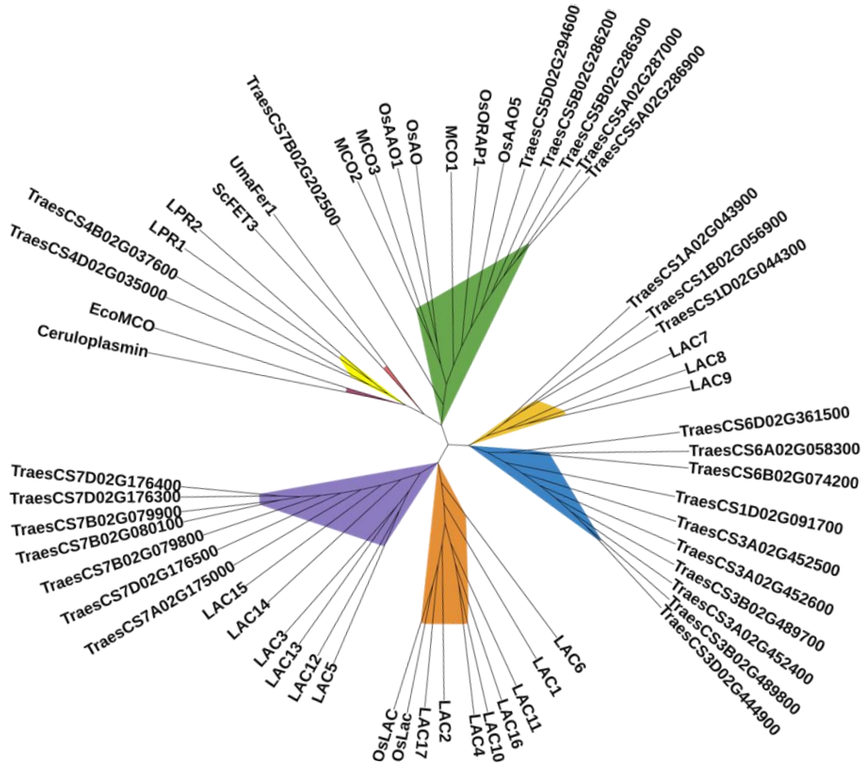
TraesCS7B02G202500
MCO2
MCO3
OsAAO1
OsAO
MCO1
OsORAP1
OsAAO5
TraesCS5D02G294600
TraesCS5B02G286200
TraesCS5B02G286300
TraesCS5A02G287000
TraesCS5A02G286900
UmaFer1
ScFET3
LPR2
LPR1
TraesCS4B02G037600
TraesCS4D02G035000
EcoMCO
Ceruloplasmin
TraesCS1A02G043900
TraesCS1B02G056900
TraesCS1D02G044300
LAC7
LAC8
LAC9
TraesCS6D02G361500
TraesCS6A02G058300
TraesCS6B02G074200
TraesCS1D02G091700
TraesCS3A02G452500
TraesCS3A02G452600
TraesCS3B02G489700
TraesCS3A02G452400
TraesCS3B02G489800
TraesCS3D02G444900
TraesCS7D02G176400
TraesCS7D02G176300
TraesCS7B02G079900
TraesCS7B02G080100
TraesCS7B02G079800
TraesCS7D02G176500
TraesCS7A02G175000
LAC15
LAC14
LAC3
LAC13
LAC12
LAC5
OsLAC
OsLac
LAC17
LAC2
LAC4
LAC10
LAC16
LAC11
LAC1
LAC6

(B)

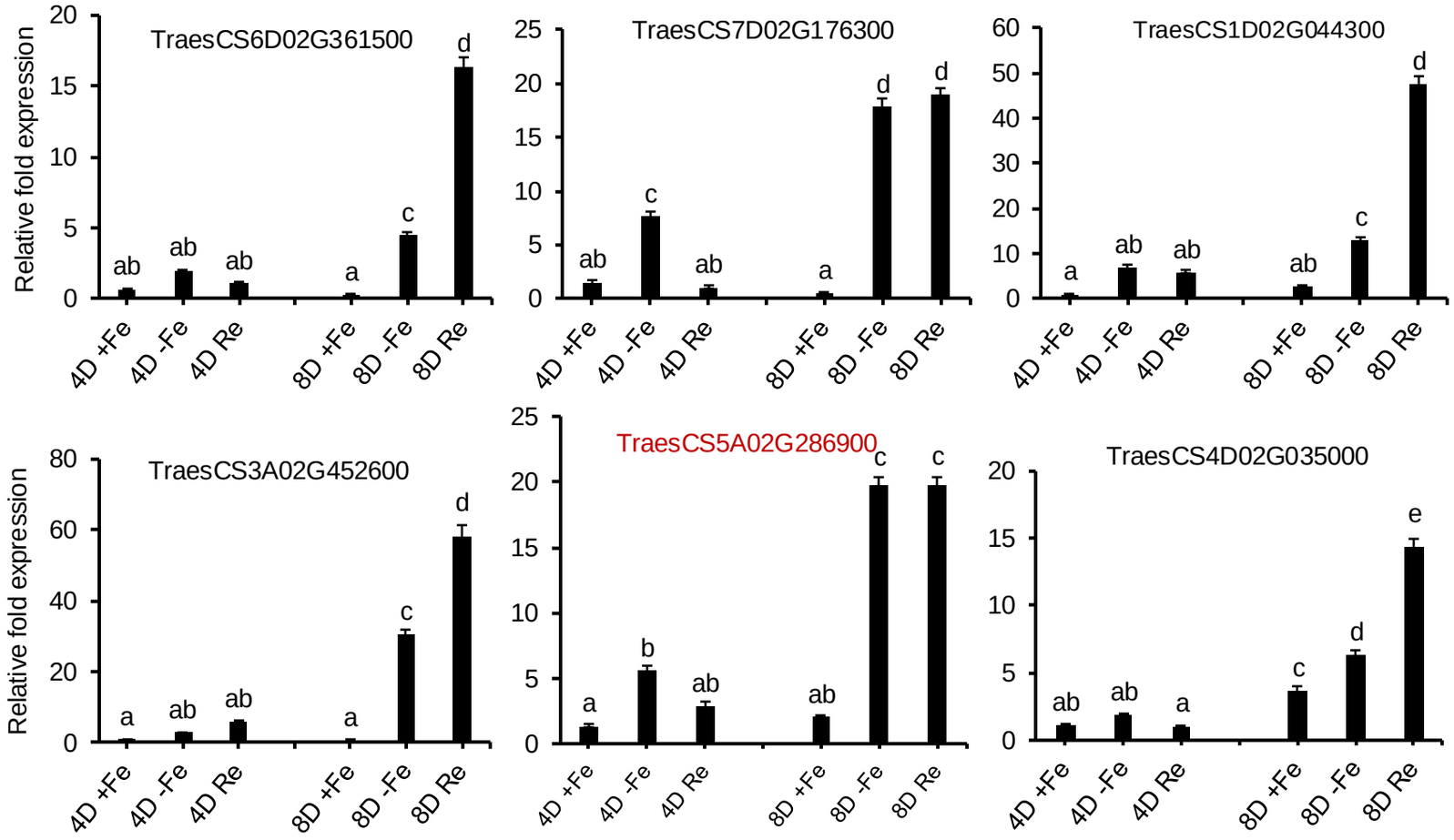
TraesCS6D02G361500
TraesCS7D02G176300
TraesCS1D02G044300
TraesCS3A02G452600
TraesCS5A02G286900
TraesCS4D02G035000
Relative fold expression
4D +Fe
4D -Fe
4D Re
8D +Fe
8D -Fe
8D Re

Figure 4

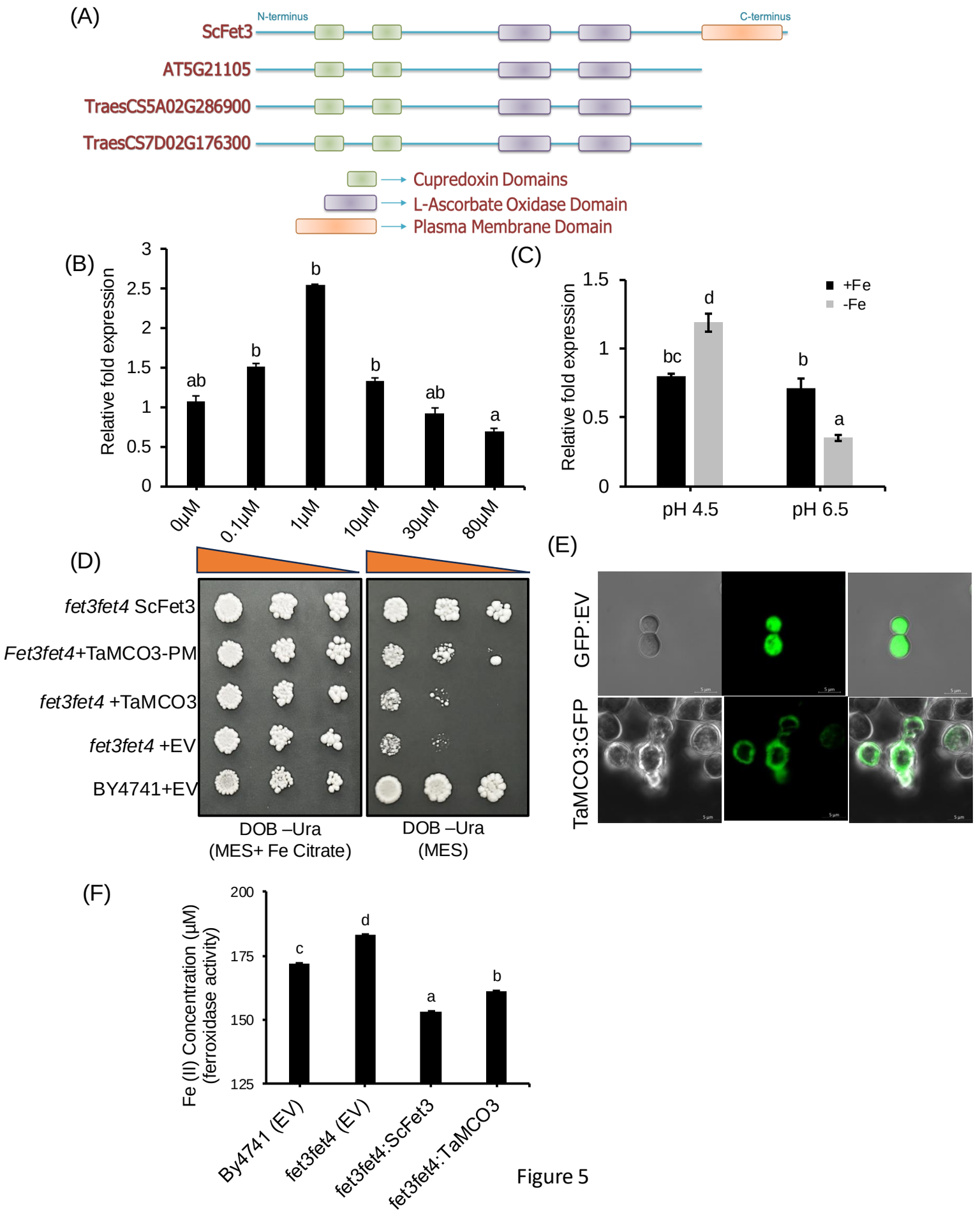
(A)
N-terminus
C-terminus
ScFet3
AT5G21105
TraesCS5A02G286900
TraesCS7D02G176300
Cupredoxin Domains
L-Ascorbate Oxidase Domain
Plasma Membrane Domain
(B)
Relative fold expression
0μM
0.1μM
1μM
10μM
30μM
80μM
(C)
+Fe
-Fe
pH 4.5
pH 6.5
(D)
fet3fet4 ScFet3
Fet3fet4+TaMCO3-PM
fet3fet4 +TaMCO3
fet3fet4 +EV
BY4741+EV
DOB –Ura
(MES+ Fe Citrate)
DOB –Ura
(MES)
(E)
GFP:EV
TaMCO3:GFP
(F)
Fe (II) Concentration (μM)
(ferroxidase activity)
By4741 (EV)
fet3fet4 (EV)
fet3fet4:ScFet3
fet3fet4:TaMCO3

Figure 5

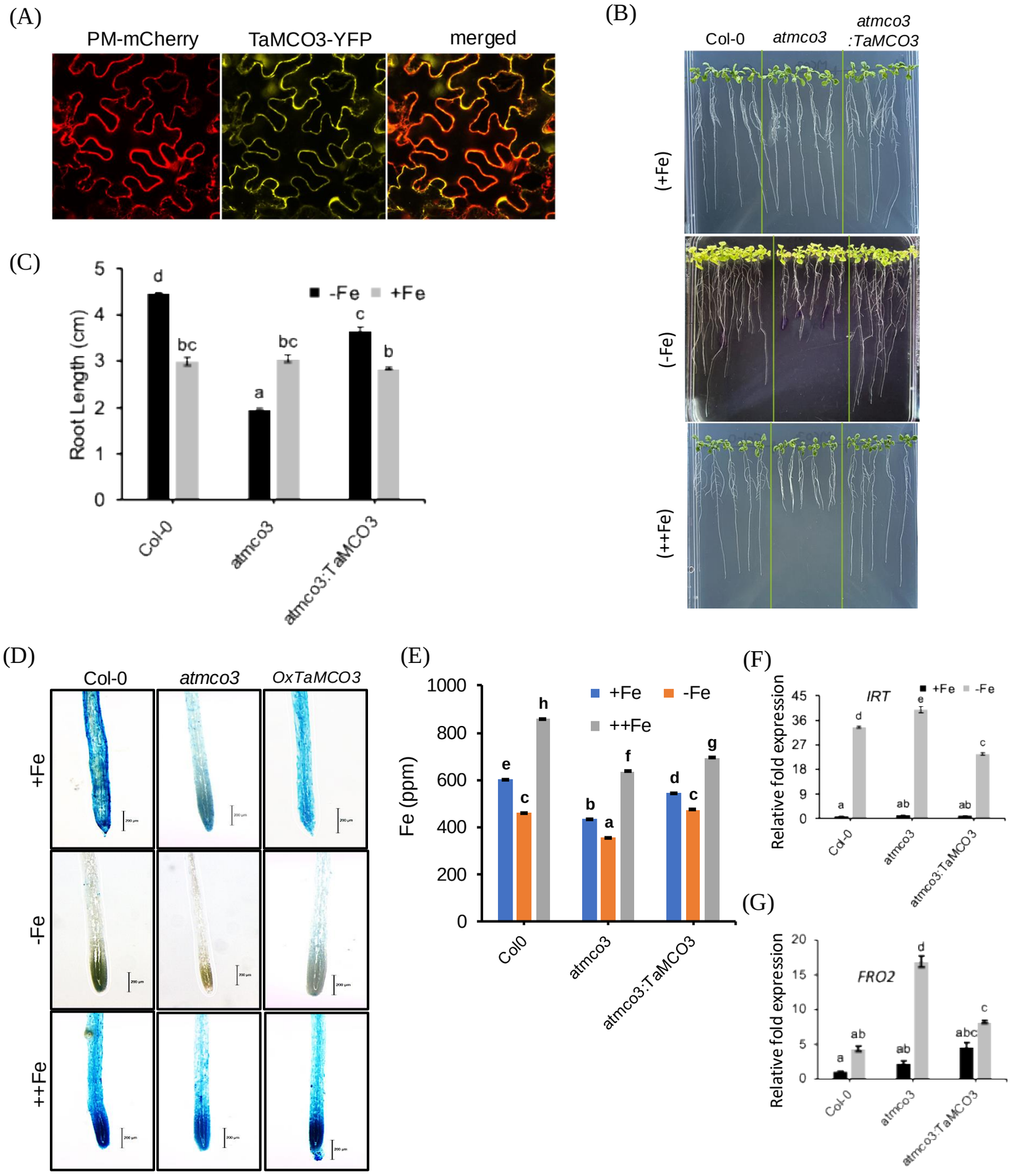
(A)
PM-mCherry
TaMCO3-YFP
merged
(B)
Col-0
atmco3
atmco3 :TaMCO3
(+Fe)
(-Fe)
(++Fe)
(C)
-Fe
+Fe
Root Length (cm)
Col-0
atmco3
atmco3:TaMCO3
(D)
Col-0
atmco3
OxTaMCO3
+Fe
-Fe
++Fe
(E)
+Fe
-Fe
++Fe
Fe (ppm)
Col0
atmco3
atmco3:TaMCO3
(F)
IRT
+Fe
-Fe
Relative fold expression
Col-0
atmco3
atmco3:TaMCO3
(G)
FRO2
Relative fold expression
Col-0
atmco3
atmco3:TaMCO3

Figure 6

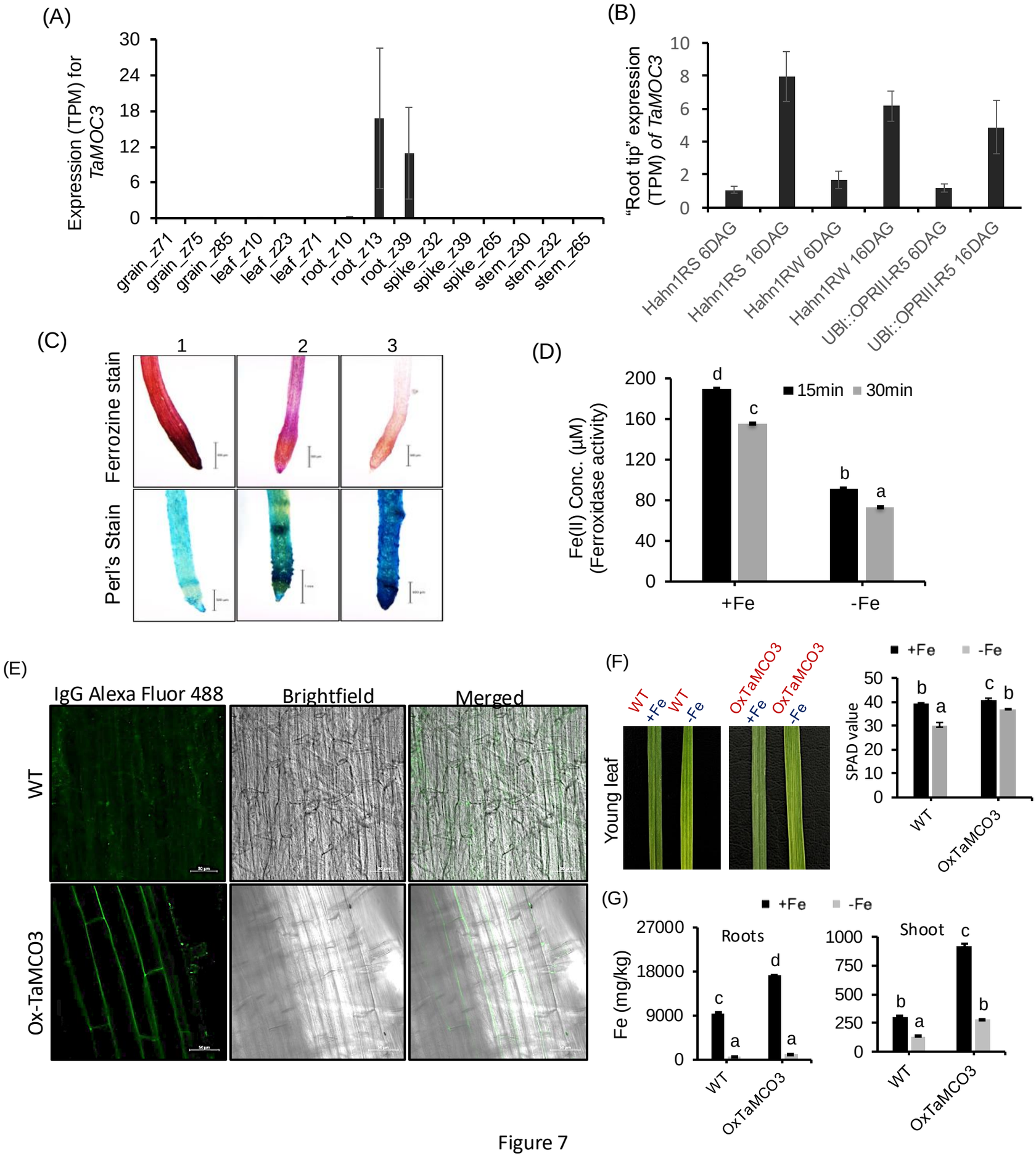
(A)
Expression (TPM) for TaMOC3
30
24
18
12
6
0
grain_z71
grain_z75
grain_z85
leaf_z10
leaf_z23
leaf_z71
root_z10
root_z13
root_z39
spike_z32
spike_z39
spike_z65
stem_z30
stem_z32
stem_z65
(B)
"Root tip" expression (TPM) of TaMOC3
10
8
6
4
2
0
Hahn1RS 6DAG
Hahn1RS 16DAG
Hahn1RW 6DAG
Hahn1RW 16DAG
UBI::OPRIII-R5 6DAG
UBI::OPRIII-R5 16DAG
(C)
1
2
3
Ferrozine stain
Perl's Stain
(D)
Fe(II) Conc. (µM) (Ferroxidase activity)
200
160
120
80
40
0
15min
30min
d
c
b
a
+Fe
-Fe
(E)
IgG Alexa Fluor 488
Brightfield
Merged
WT
Ox-TaMCO3
(F)
WT +Fe
WT -Fe
OxTaMCO3 +Fe
OxTaMCO3 -Fe
Young leaf
+Fe
-Fe
SPAD value
50
40
30
20
10
0
b
a
c
b
WT
OxTaMCO3
(G)
+Fe
-Fe
Roots
Fe (mg/kg)
27000
18000
9000
0
c
a
d
a
WT
OxTaMCO3
Shoot
1000
750
500
250
0
b
a
c
b
WT
OxTaMCO3

Figure 7

(A)

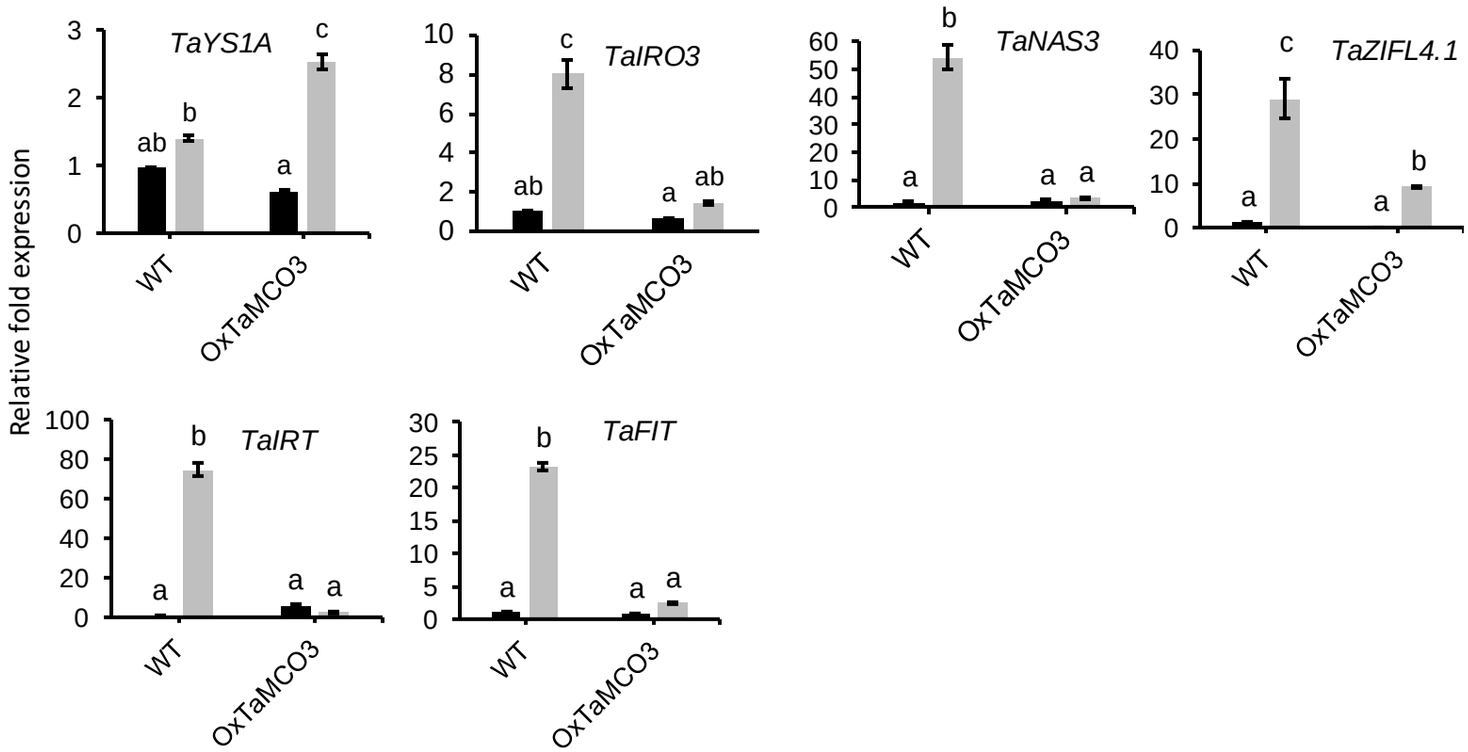
Relative fold expression
TaYS1A
TaIRO3
TaNAS3
TaZIFL4.1
TaIRT
TaFIT
WT
OxTaMCO3

(B)

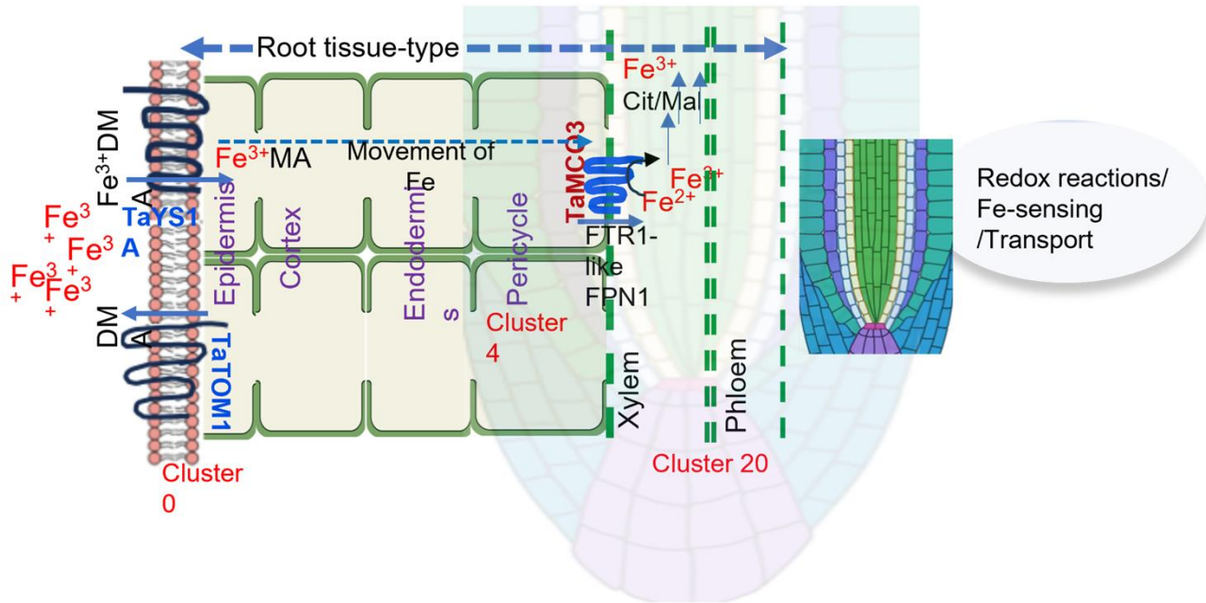
Root tissue-type
Movement of Fe
Epidermis
Cortex
Endodermis
Pericycle
Xylem
Phloem
TaYS1
TaTOM1
TaMCO3
FTR1-like
FPN1
Cit/Mal
Cluster 0
Cluster 4
Cluster 20
Redox reactions/
Fe-sensing
/Transport

Figure 8